	<p><i>Multilayer Coatings for High-Energy Optics for Astrophysics</i></p> <p>Results of tests performed at PANTER and INAF/OAB on the X-ray optic 349 manufactured at MSFC and Harvard-CfA</p>					
Code:02/07	INAF/OAB Technical Report	Issue: 1	Class	CONFIDENTIAL	Page: 1	1

Multilayer Coatings for High-Energy Optics for Astrophysics

Results of tests performed at PANTER and INAF/OAB on the X-ray optic 349 manufactured at MSFC and Harvard-CfA

*Issued by **D. Spiga** (INAF/OAB, Merate, Italy)*

*Data reduction and interpretation by **D. Spiga** and **R. Canestrari** (INAF/OAB, Merate, Italy)*

*Mirror shells electroformed by MSFC/NASA (Huntsville, AL, USA) under supervision of **B. Ramsey***

*Multilayer coating deposited at the Harvard – Smithsonian Center for Astrophysics (Boston, MA, USA) by **S. Romaine**, **P. Gorenstein**, **R. Bruni***


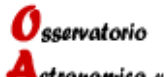
*Mirror shell integration by **S. Basso**, **F. Mazzoleni**, **R. Valtolina** (INAF/OAB)*

*X-ray measurements performed by PANTER (MPE, Garching, Germany) team - **M. Freyberg**, **W. Burkert**, **G. Hartner**, **B. Budau**.*

*PROMAP and AFM measurements performed at **G. Destefanis** and **D. Colombo**, (MEDIA-LARIO TECHN., Bosisio Parini, Italy)*


*LTP measurements by **M. Gubarev** (MSFC/NASA)*

*Reviewed by **G. Pareschi** (INAF/OAB)*

 	<p><i>Multilayer Coatings for High-Energy Optics for Astrophysics</i></p> <p>Results of tests performed at PANTER and INAF/OAB on the X-ray optic 349 manufactured at MSFC and Harvard-CfA</p>						
Code:02/07	INAF/OAB Technical Report	Issue:	1	Class	CONFIDENTIAL	Page:	2

Contents

1. Aim of the document.....	4
2. Optic 349 - shell HXT 150: results of tests at PANTER and INAF/OAB.....	5
2.1 – PANTER results: effective areas	6
2.2 – PANTER results: Half Energy Widths	7
2.3 – X-ray tests at INAF/OAB	8
2.4 – Topographical analysis (LTP, PROMAP, WYKO and AFM)	10
2.4.1 – LTP	10
2.4.2 – PROMAP 40×	10
2.4.3 – WYKO 20×	11
2.4.4 – AFM (2 μm)	11
2.5 – Final PSD - interpretation of the HEW trend	12
3. Optic 349 - HXT 230: results of tests at PANTER and INAF/OAB.....	15
3.1 – Witness mirror sample: X-ray reflectivity tests	15
3.2 – PANTER results: effective areas	17
3.3 – PANTER results: Half Energy Widths	18
3.4 – X-ray tests at INAF/OAB	19
3.5 – Topographical analysis (PROMAP, WYKO and AFM)	20
3.5.1 – PROMAP 40×	20
3.5.2 – WYKO 20×	21
3.5.3 – AFM (2 μm)	22
3.6 – Final PSD - HEW trend interpretation	22
4. Mirror shells HXT 150 + 230: overall optic properties	24
4.1 – PANTER results: effective areas	25
4.1.1 – Experimental results	25
4.1.2 – Interpretation of effective areas	25
4.2 – PANTER results: Half Energy Widths	28
5. A comparison of the optics PSD and HEW	30
5.1 Optics 346 (HXT230) and 349 (HXT150 and HXT230)	30
5.2 Comparison of HXT230 mirror shells (335, 346, 349 HXT230)	31

	<p><i>Multilayer Coatings for High-Energy Optics for Astrophysics</i></p> <p>Results of tests performed at PANTER and INAF/OAB on the X-ray optic 349 manufactured at MSFC and Harvard-CfA</p>					
Code:02/07	INAF/OAB Technical Report	Issue: 1	Class	CONFIDENTIAL	Page: 3	

Applicable Documents


- [AD1] D. Spiga et al., *Optic (HXT 150 + 230) test at PANTER facility: Preliminary Performances Evaluation and Proposed Test Plan Definition*, **INAF/OAB Internal Report 03/06**
- [AD2] D. Spiga et al., *X-ray optic 346 manufactured at MSFC and Harvard-CfA: results of tests at PANTER facility and surface characterization*, **INAF/OAB Internal Report 01/07**

Reference Documents

- [RD1] S. Romaine et al., *Development of a prototype Nickel Optic for the Constellation-X Hard X-ray telescope: IV* - **SPIE Proc.** 6266 p. 62661C
- [RD2] H. Bräuninger et al., *Calibration of hard X-ray (15 – 50 keV) optics at the MPE test facility PANTER* - **SPIE Proc.** 5168, p. 283-293
- [RD3] D. Spiga et al., *Characterization of multilayer stack parameters from X-ray reflectivity data using the PPM program: measurements and comparison with TEM results* - **SPIE Proc.** 6266 p. 626616
- [RD4] D. Spiga, *Analytical evaluation of the X-ray scattering contribution to imaging degradation in grazing-incidence X-ray telescopes*, **Astronomy and Astrophysics**, Vol. 468, issue 2, pp. 775-784

Acronyms

CCD	Charge-Coupling Device
HEW	Half-Energy Width
EA	Effective Area
f.c.	For comparison
FF	Flat Field
HXT	Hard X-ray Telescope
INAF	Istituto Nazionale di AstroFisica / <i>Italian Institute for Astrophysics</i>
MPE	Max-Planck Institut für Extraterrestrische Physik / <i>Max Planck Institute for Extraterrestrial Physics</i>
MSFC	Marshall Space Flight Center
OAB	Osservatorio Astronomico di Brera / <i>Brera Astronomical Observatory</i>
PSD	Power Spectral Density
PSPC	Position-Sensitive Proportional Counter
ROI	Region Of Interest
UV	UltraViolet

	<p><i>Multilayer Coatings for High-Energy Optics for Astrophysics</i></p> <p>Results of tests performed at PANTER and INAF/OAB on the X-ray optic 349 manufactured at MSFC and Harvard-CfA</p>				
Code:02/07	INAF/OAB Technical Report	Issue: 1	Class	CONFIDENTIAL	Page: 4

1. Aim of the document

Aim of this document is to present the results of X-ray tests performed at the PANTER facility in full illumination setup, onto a X-ray optic prototype (named **349** in the following) formed by *two confocal Wolter I mirror shells*. The largest shell (**HXT 230** heretofore) had a 230 mm diameter and an on-axis incidence angle of 0.164 deg, whereas the smallest one (**HXT 150**) was a 150 mm diameter one with an on-axis incidence angle of 0.107 deg.

Both mirror shells (with a nominal focal length of 10 m) were manufactured by mandrel replication at MSFC by electroforming with a special Ni/Co alloy. Then the HXT230 mirror shell was coated with a W/Si graded multilayer by DC magnetron sputtering at the *Harvard-CfA* [RD1] in order to endow it with a larger reflectivity in hard X-rays. The HXT 150 was not multilayer-coated because the Ni substrate, with such a small incidence angle, was sufficient to reflect up to 30 keV in total external reflection regime.

The two mirror shells were assembled in a mechanical case at INAF/OAB (see Fig. 1). Then, the optic has been mounted in a special manipulator (developed at INAF/OAB) to handle the rotation/tilt of the optic, because due to the long focal length the optic had to be mounted in the vacuum tube of PANTER and the usual PANTER manipulator could not be used [RD1, RD2]. The INAF/OAB manipulator is also equipped with a system of two independent shutters to measure the incident X-ray flux *or* the focused beam by the two mirror shells, separately and together.

The test planning was described in [AD1]. For an accurate description of the PANTER facility, see [RD2]. Essential results are also reported in [RD1]. For the data reduction procedure, we will also refer to [AD2].

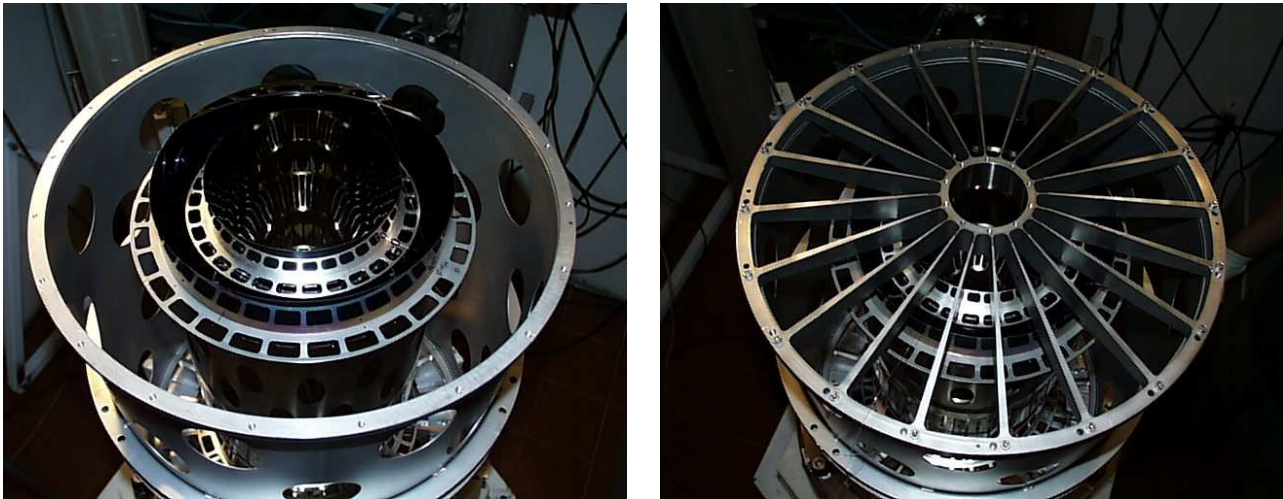



Fig. 1: The optic 349 during the integration: the two shells are clearly visible. (left) Upper spider open. (right) Upper spider closed. Note the stiffening rings used to minimize the shells deformation during the mounting. The rings have been released after the glue polymerization, and fixed to the spider arms.

	<p align="center"><i>Multilayer Coatings for High-Energy Optics for Astrophysics</i></p> <p align="center">Results of tests performed at PANTER and INAF/OAB on the X-ray optic 349 manufactured at MSFC and Harvard-CfA</p>				
Code:02/07	INAF/OAB Technical Report	Issue: 1	Class	CONFIDENTIAL	Page: 5


2. Optic 349 - shell HXT 150: results of tests at PANTER and INAF/OAB

The mirror shell HXT 150 has not been coated, i.e., reflects X-rays in total external reflection with the Nickel surface of the shell itself. The incidence angle is a small one (0.107 deg, as seen from infinity): this allows the reflection of X-rays in total external reflection regime up to 30 keV, even though the finite distance of the source limits in this case the reflection band to a maximum photon energy of 25 keV.

We list in Tab. 1 the geometrical features of this mirror shell. Notice the much larger obscured area fraction by the spider (21 %) than for the mirror shell tested in [AD2] (10 %). This is due to the adoption of small Al rods (4.8 mm large, 1.95 mm thick), that were bonded to the spider at the optic front-end. These rods are slightly larger than the spider arms in order to shade their lateral surface, avoiding the X-ray scattering from the spider arms, that are not optically-polished. The X-ray transparency of these rods as a function of the energy is plotted in Fig. 2. The variation of the transmitted flux though the Al rods has been included in the effective area simulations.

Tab.1: geometrical features of the mirror shell HXT 150

<i>Parameter</i>	<i>symbol</i>	<i>Value</i>
maximum mirror diameter (parabola)	$2R_{max}$	150.8 mm
median mirror diameter	$2R_{med}$	150.0 mm
minimum mirror diameter (hyperbola)	$2R_{min}$	147.6 mm
mirror length (parabola + hyperbola)	$2L$	426 mm
on-axis incidence angle	α	0.1068°
focal length (for a source at infinity)	f	10000 ± 3 mm
mirror walls thickness	τ	100 μm
Geometric cross-section from infinity	A	1.87 cm ²
Beam divergence (at the mirror front-end)	θ	0.0357°
Actual incidence angle on the parabola	α_{par}	0.1425°
Actual incidence angle on the hyperbola (for <i>double reflection</i>)	α_{hyp}	0.0711°
Actual image-mirror distance	X_i	10.9 m
<i>Lost</i> area fraction of parabola for double reflection	Q	49.6%
Obscured area fraction by spider (low energies)	V	10-21 %
Radius of the parabola single-reflection corona	r_p	27.5 mm
Radius of the hyperbola single-reflection corona	r_h	53.7 mm
Geometric cross-section for parabola single reflection, spider vignetted	A_G^{par}	0.99 cm ²
<i>Geometric cross-section for double reflection, spider vignetted</i> (1 keV) A_G^{hp}		1.01 cm ²

	<p align="center"><i>Multilayer Coatings for High-Energy Optics for Astrophysics</i></p> <p align="center">Results of tests performed at PANTER and INAF/OAB on the X-ray optic 349 manufactured at MSFC and Harvard-CfA</p>					
Code:02/07	INAF/OAB Technical Report	Issue: 1	Class	CONFIDENTIAL	Page: 6	

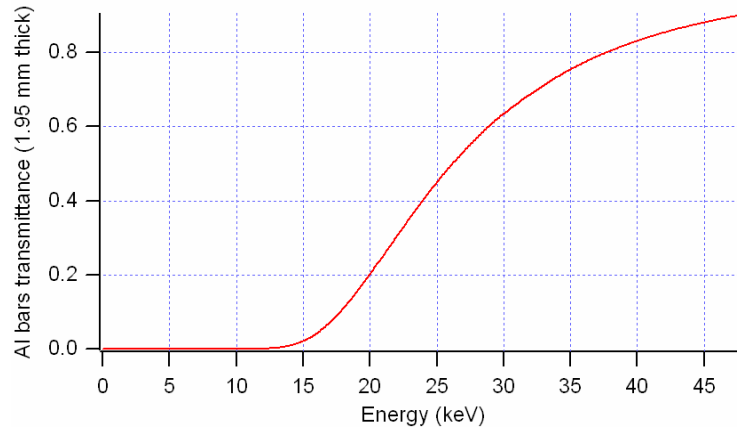


Fig. 2: the X-ray transmittance of the Al rods used to avoid the X-ray scattering at low energy from the lateral surface of the spider arms.

2.1 – PANTER results: effective areas

The EA of the HXT 150 was measured, as in previous calibrations, with both the PSPC (low energies) and the pn-EPIC (high energies) detector. Some images derived from pn-EPIC data are shown in Fig. 3, whereas the effective area as function of the photon energy is plotted in Fig. 4, superposed to some reflectivity models, with different possible roughness values of the surface. In order to compute the EA, a circular ROI of 88 pixels (250 arcsec) radius was adopted for both PSPC and pn-EPIC (it is the largest allowed circular ROI for the pn-EPIC, with the adopted positioning of the focal spot).

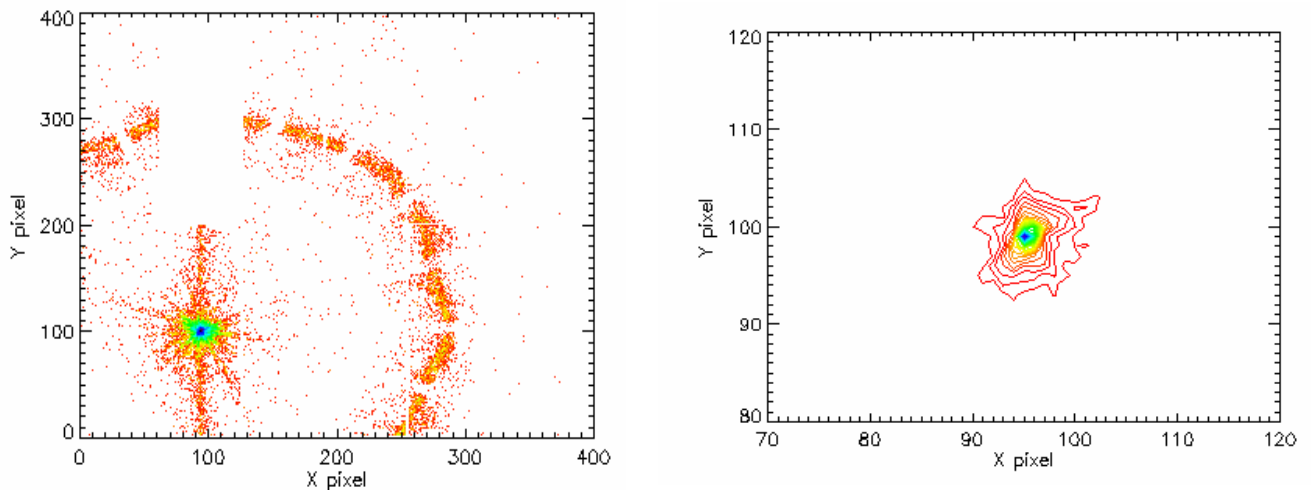



Fig. 3: reconstruction of the pn-EPIC field of the reflection of the mirror shell HXT 150. (left) the full pn-EPIC field between 15 and 30 keV, in the 30 kV source setup.(right) closer view on the focal spot, contour plot. Compare the more regular shape with that shown in [AD2].

	<p style="text-align: center;"><i>Multilayer Coatings for High-Energy Optics for Astrophysics</i></p> <p style="text-align: center;">Results of tests performed at PANTER and INAF/OAB on the X-ray optic 349 manufactured at MSFC and Harvard-CfA</p>				
Code:02/07	INAF/OAB Technical Report	Issue: 1	Class	CONFIDENTIAL	Page: 7

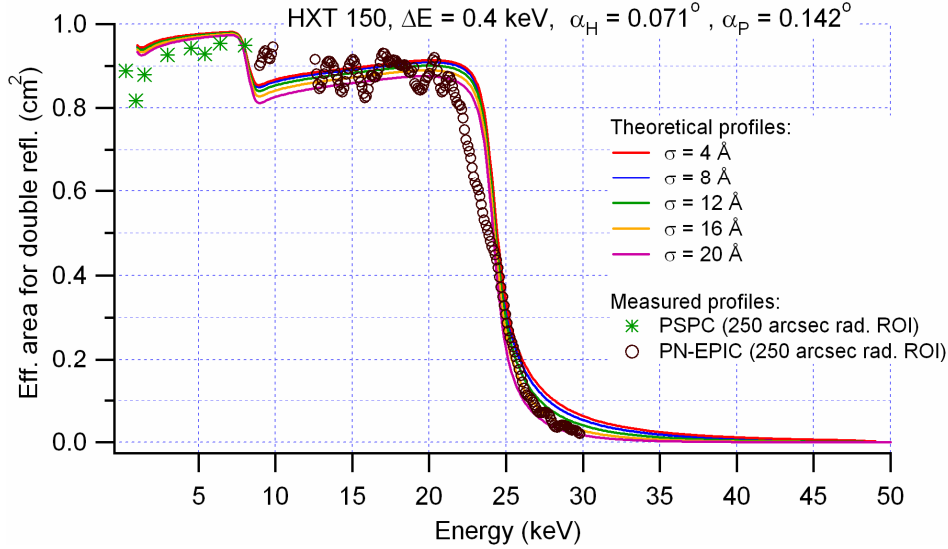


Fig. 4: mirror shell **HXT 150 effective area (EA)** for double reflection as function of energy at the PANTER facility from 0.5 to 50 keV. A constant energy resolution of 0.4 keV is assumed. Part of the increasing trend in the models from 10 to 23 keV is due to the increasing transmission of the Al bars used to screen the lateral sides of the arms of the spider (see Fig. 2). The oscillations in that energy range lie within the measurement error due to photon statistics.


EA results measured with the pn-EPIC camera are obtained from three exposures to the incident photon flux at 10, 20, 30 kV setup of the X-ray source. The overlapping energy ranges return EA values in good agreement, within the experimental error: the oscillations in the range 10-20 keV are due to the photon statistics. The measured EA is consistent with 20 Å rms, but the close spacing of model curves makes the evaluation difficult: however, from the deviation of the experimental curve from models in the vicinities of the critical energy (25 keV) we can infer the presence – as expected - of a Ni oxide layer. From the fit – not shown here – we can derive a 6.5 g/cm³ density for the Ni_xO_y layer. The thickness of the oxide layer can be estimated in 10 nm.

EA data at low X-ray energies underestimate the expected values. This can be due to the high-scattering angle of low-energy photons (scattered at angles larger than 250 arcsec).

2.2 – PANTER results: Half Energy Widths

Fig. 5 summarizes the HEW values measured for the HXT 150 in the energy range 0.3 – 27 keV, within a circular region of 250 arcsec radius. We also show the error bars computed from the PSF photon count statistics and from the uncertainty in the position due to the finite pixel size (2.8 arcsec: however, the HEW were computed by interpolation of the EE: this procedure returns a smaller error than the pixel size). Each HEW value is evaluated in a 2 keV-wide energy band, at intervals of 2 keV. Data between 9 and 14 keV are missing due to the used Ti filters, needed to reduce the pileup in the pn-EPIC detector.

The HEW values were computed in all the available exposures. In the overlapping regions of the spectra the HEW values are in agreement within 2 arcsec, i.e. slightly larger than the estimated error for the HEW. Moreover, the HEW is slightly larger in the 30 kV exposure where it overlaps the one at 20

	<p align="center"><i>Multilayer Coatings for High-Energy Optics for Astrophysics</i></p> <p align="center">Results of tests performed at PANTER and INAF/OAB on the X-ray optic 349 manufactured at MSFC and Harvard-CfA</p>				
Code:02/07	INAF/OAB Technical Report	Issue: 1	Class	CONFIDENTIAL	Page: 8

kV. This can be due to a small amount of Compton scattering in the pn-EPIC detector for the setup at higher energies: in fact, the amount of contribution to Compton Scattering at 25-30 keV can be roughly estimated to be 1 – 1.5 arcsec [AD2]. Owing to the variation of the reflected spectrum within the 2 keV-wide bins adopted for the calculation, the HEW values have been plotted vs. the energy centroid in each bin, as computed from the measured spectrum. We can observe a moderate increase in the HEW from 26 arcsec to 29 arcsec in the low-energy domain, afterwards the HEW is more or less constant around 32 arcsec. The behaviour beyond 26 keV is unknown, due to the decay of reflectivity after the critical energy (for the parabola). An extrapolation to $E \rightarrow 0$ aimed at the determination of the figure error HEW returned 25 arcsec, even if the HEW trend at low energies is not regular.

The smaller HEW values, with respect to the shell 346 (from 30 to 40 arcsec in the same photon energy range, see [AD2]) could be due to:

- the smaller radius that helps keeping the nominal mirror shape
- the smaller incidence angles, that helps reducing the grazing-incidence X-ray scattering.

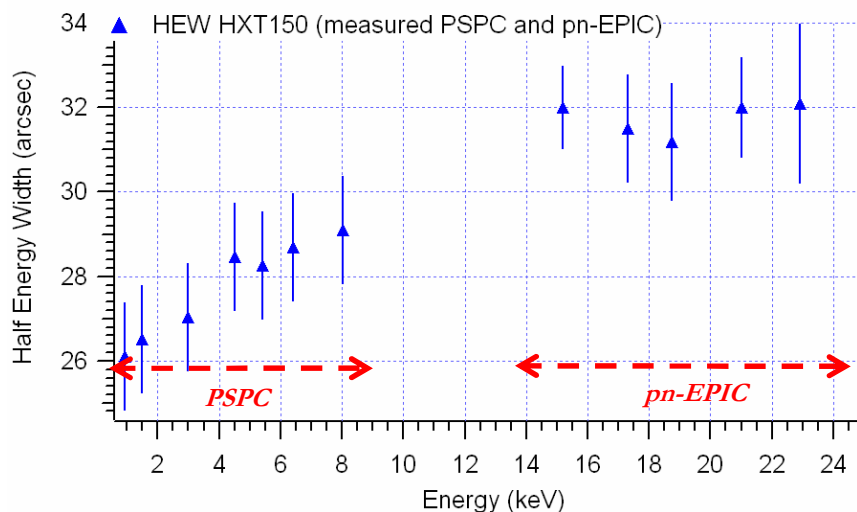



Fig. 5: measured values of the mirror shell **HXT 150** Half Energy Width, measured with the PSPC at low energies and with the pn-EPIC camera at high energies. The detector spatial resolution of the PSPC was subtracted in quadrature from data. The finite pixel size of the pn-EPIC was ruled out by the interpolation of PSF data.

2.3 – X-ray tests at INAF/OAB

X-ray tests were performed at INAF/OAB on some small pieces of the mirror shell HXT 150 in order to confirm the results achieved at PANTER. In Fig. 6 (top) we show the measured XRR of a piece of the HXT 150 mirror shell at 8.05 keV. The mirror shell piece had a 10 x 10 cm size, much larger than the X-ray beam size in use (1 cm height, 70 μ m width). In spite of the small lateral size of the beam, the irregularities of the surface prevented any measurement at angles smaller than 600 arcsec. Also a small fraction of the incident beam can be lost up to 1500 arcsec. The window in front of the detector had a width of 2 mm, at a distance of 340 mm from the center of the sample. This corresponds to an acceptance angle of 1200 arcsec, more than twice the adopted one at PANTER (500 arcsec).

	<p align="center"><i>Multilayer Coatings for High-Energy Optics for Astrophysics</i></p> <p align="center">Results of tests performed at PANTER and INAF/OAB on the X-ray optic 349 manufactured at MSFC and Harvard-CfA</p>				
Code:02/07	INAF/OAB Technical Report	Issue: 1	Class	CONFIDENTIAL	Page: 9

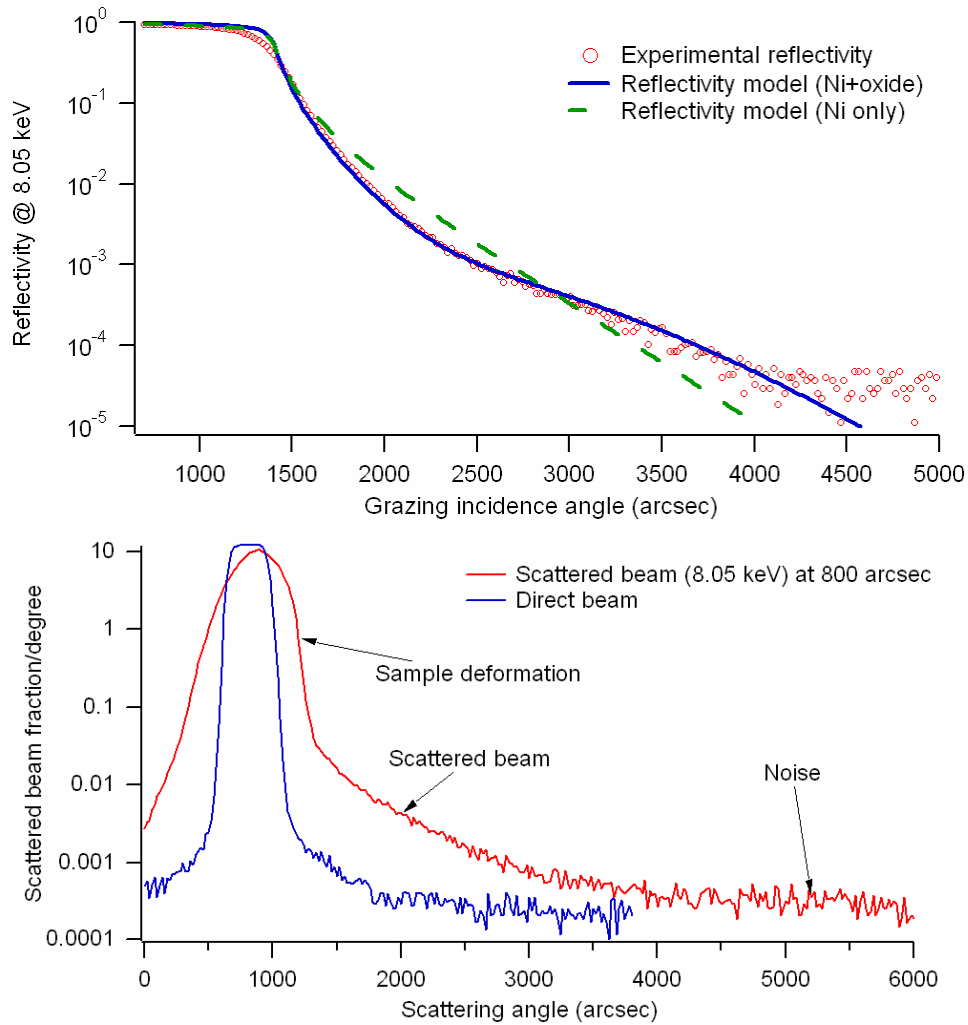


Fig. 6: X-ray analysis (8.05 keV) of a sample of the HXT150 mirror shell. XRR (above) and XRS (bottom) in total external reflection regime, at an incidence angle of 1040 arcsec.

A simple substrate of Ni would not explain the measured reflectivity (the dashed line): a clear evidence of a Ni oxide layer (4 nm thick, with a density value of 6.5 g/cm^3) can be inferred over the Ni structure (solid line). The presence of a layer with this density (but 3 times thicker) was evident also from the PANTER data (see Fig. 4). The roughness rms inferred is $12 \div 13 \text{ \AA}$ for both oxide and Ni substrate. These values are related to the set of incidence angles of the scan and to the angular acceptance of the detector: in fact, as the better agreement experiment – model is reached at $\theta_i = 3000 \text{ arcsec}$, we could easily compute that this σ value is referred to all the spatial wavelengths smaller than 3.3 \mu m , i.e. in the AFM sensitivity range (see Sect. 2.4.4), that returns an average σ of 12 \AA , in good agreement with the XRR.

		<p><i>Multilayer Coatings for High-Energy Optics for Astrophysics</i></p> <p>Results of tests performed at PANTER and INAF/OAB on the X-ray optic 349 manufactured at MSFC and Harvard-CfA</p>				
Code:02/07	INAF/OAB Technical Report	Issue: 1	Class	CONFIDENTIAL	Page: 10	

XRS measurements were performed in total external reflection regime (see Fig. 6, right) at 800 and 1100 incidence angles. The measurement was made difficult by a relevant deformation of the sample, but a clear X-ray scattering is visible and allowed the measurement of PSD between 10 and 1 μm spatial wavelengths (see Fig. 10). The PSD is consistent with the AFM and the WYKO data, the slightly smaller values of the PSD could indicate a slight better smoothness of the Ni substrate with respect to the outer Ni oxide surface.

2.4 – Topographical analysis (LTP, PROMAP, WYKO and AFM)

2.4.1 – LTP

LTP measurements of the longitudinal profile of the mirror shell were taken at MSFC with the mirror shell mounted in the integration case to avoid deformations of the shell. The profiles exhibit variable deviations from the nominal profile (some microns), especially at the mirror end, where they are fixed to the spider. The high-frequency behaviour has been analyzed in terms of PSD (see Fig. 10), after a subtraction of a high-order polynomial from rough profiles: the profiles of the parabolic surface have been excluded from the PSD computation because only $\frac{1}{2}$ parabolic surface is involved in the reflection.

2.4.2 – PROMAP 40×

The PROMAP 40x measurements (performed at *Media-Lario techn.*), covers a spectral range from $\sim 100\ \mu\text{m}$ down to $0.3\ \mu\text{m}$. One of the PROMAP surface map is shown in Fig. 7: the surface is covered by *scratches* (0.5 nm deep), preferentially oriented in the y direction (the optical axis). Also a *large number of holes* (in blue) are present, with a distribution in size around some μm , and a few nm depth. In addition, a *lower number of peaks* can be observed: they are a few 10 nm high and some μm wide.

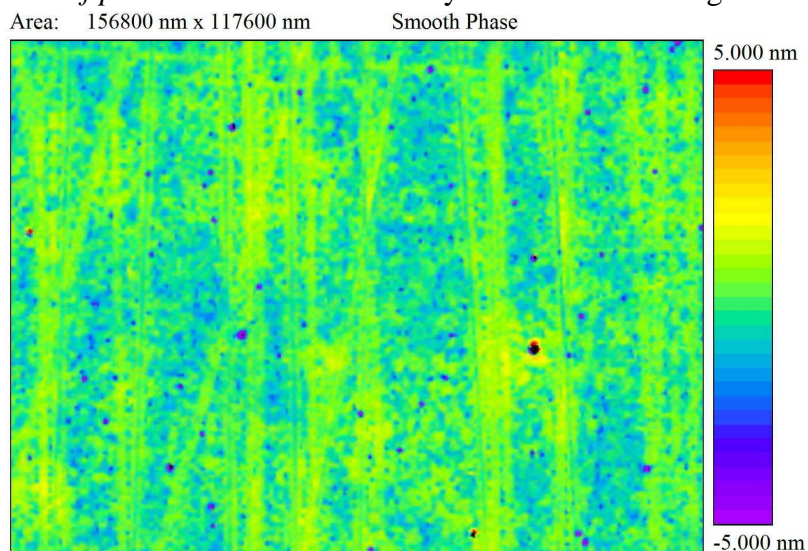



Fig. 7: a PROMAP image of the HXT150 flattened surface (courtesy by Media-Lario techn.). The topography is characterized by scratches (mainly in the optical axis direction) and point-like defects (mainly holes).

	<p align="center"><i>Multilayer Coatings for High-Energy Optics for Astrophysics</i></p> <p align="center">Results of tests performed at PANTER and INAF/OAB on the X-ray optic 349 manufactured at MSFC and Harvard-CfA</p>					
Code:02/07	INAF/OAB Technical Report	Issue: 1	Class	CONFIDENTIAL	Page: 11	

The images were analyzed computing the PSD in both (x and y) directions. The one that is interesting is the PSD along y since the incidence plane of X-rays lies in the optical axis direction, but the two PSDs are not too different (less than 0.5 Å) because the scratches have a limited depth when compared to that of holes. All peaks larger than 30 nm (probably contaminations) were excluded from the PSD computation. The average PSD is plotted in Fig. 10.

2.4.3 – WYKO 20×

WYKO 20x measurements performed at INAF/OAB cover a lower frequencies range (200 – 10 μm). They confirmed qualitatively the results of PROMAP (see an example profile in Fig. 8), even though WYKO profiles appeared quantitatively smoother at high frequencies. This is evident from the comparison of PSDs (Fig. 10): by means of a different filtering of PROMAP images, one can see that the discrepancy is due to selection effects in WYKO profiles. However, XRS data are more in agreement with WYKO.

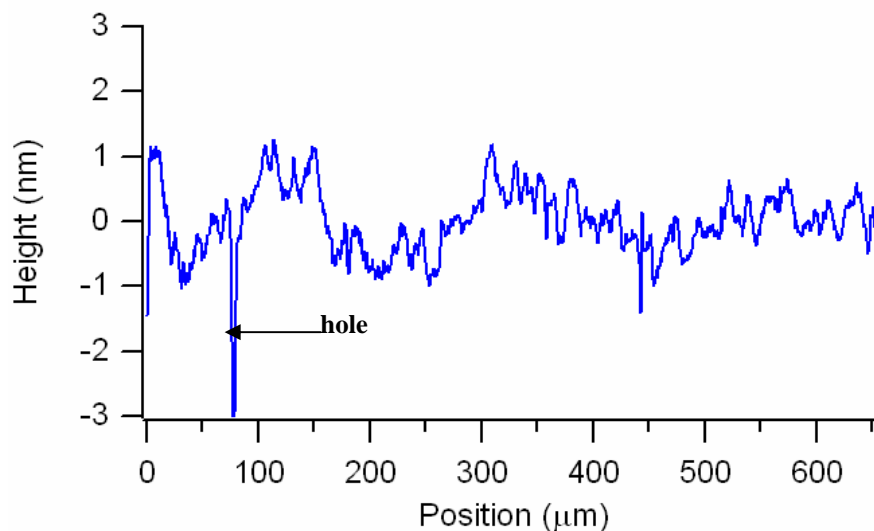



Fig. 8: a WYKO profile of the HXT150, in the direction of the optical axis.

2.4.4 – AFM (2 μm)

AFM measurements were performed at *Media-Lario techn.* using a Veeco Explorer stand-alone AFM, in non-contact mode. AFM maps cover a 2 μm x 2 μm area with a lateral resolution of 7 nm. A 3D visualization of a sampled point is shown in Fig. 9. The high-frequency content is relevant, as can be seen from the large number of peaks with several nm heights. Also some holes are present, even though they cannot be seen in the 3D visualization. The average σ of the performed measurements is 12 Å. Also the average PSD was computed from the measurements (see Fig. 10).

		<p><i>Multilayer Coatings for High-Energy Optics for Astrophysics</i></p> <p>Results of tests performed at PANTER and INAF/OAB on the X-ray optic 349 manufactured at MSFC and Harvard-CfA</p>					
Code:02/07	INAF/OAB Technical Report	Issue:	1	Class	CONFIDENTIAL	Page:	12

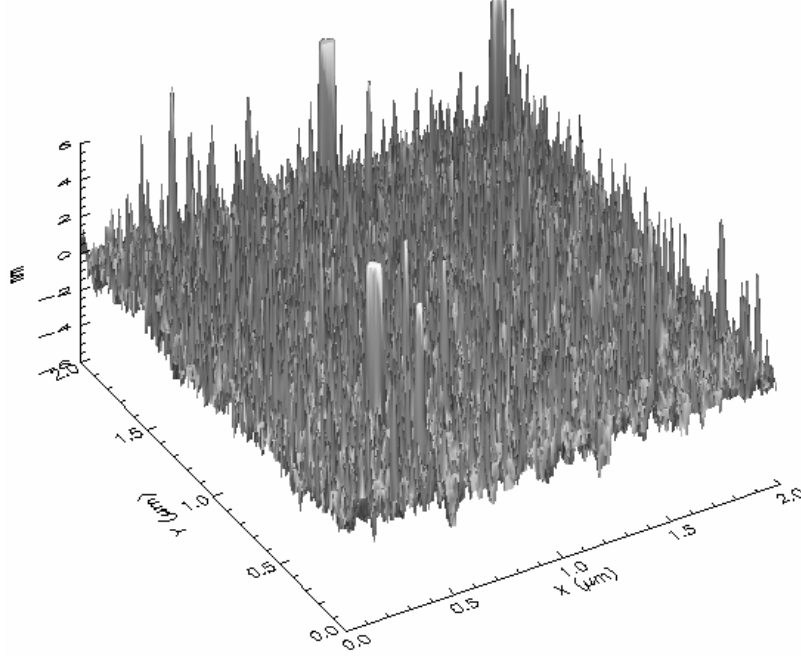


Fig. 9: an AFM map of the HXT150 mirror shell surface (courtesy by Media-Lario techn.). The rms of the surface is 13 Å.

2.5 – Final PSD - interpretation of the HEW trend


The PSD obtained from the superposition of the PSDs measured using all the available techniques is plotted in Fig. 10 (blue marks). The agreement is quite satisfactory (except for WYKO data, that underestimate the PSD). The wavelengths range 5 mm – 300 μm is, however, not characterized by the adopted techniques: a measurement with the WYKO (2.5x magnification), that would cover that range, was not possible due to the sample curvature.

The millimeter range is, indeed, well covered by the analysis of the HEW trend of the PANTER data (see Fig. 5): the HEW trend with the photon energy is, in fact, related immediately to the PSD of the surface, provided that one can have a solid estimate of the figure error HEW. Following the procedure described in [AD2] and in [RD4] one can derive the PSD of the surface from $H(\lambda)$, the XRS contribution to the HEW. The function $H(\lambda)$ is known from a subtraction in quadrature of the figure HEW:

$$HEW_{meas}^2(\lambda) \approx HEW_{fig}^2 + H^2(\lambda),$$

and the PSD can be computed from the derivative of the ratio $H(\lambda) / \lambda$ (D. Spiga, A&A):

$$\frac{P(f)}{\lambda} \frac{d}{d\lambda} \left(\frac{H(\lambda)}{\lambda} \right) = - \frac{\ln(4/3)}{4\pi^2 \sin^3 \vartheta_i},$$

	<p><i>Multilayer Coatings for High-Energy Optics for Astrophysics</i></p> <p>Results of tests performed at PANTER and INAF/OAB on the X-ray optic 349 manufactured at MSFC and Harvard-CfA</p>						
Code:02/07	INAF/OAB Technical Report	Issue: 1	Class	CONFIDENTIAL	Page:	13	

the factor $\ln(4/3)$ accounts for the double reflection: we did not account here for the beam divergence, even if it is non-negligible. The spatial frequencies f are known from the simple formula:

$$f = H(\lambda) \frac{\sin \vartheta_i}{2\lambda}.$$

The PSD computed from the HEW trend, using the exposed method, is overplotted to the topography data in Fig. 10 (red triangles). The agreement is satisfactory assuming $HEW_{fig} = 15$ arcsec figure error: larger values of HEW_{fig} can be ruled out as they would cause a mismatch of the PSD derived from the HEW. Furthermore, we can derive from the last equation and from the Debye-Waller formula a value for the roughness rms in the wavelength range $382 - 13 \mu m$: $\sigma = 11.3 \text{ \AA}$. F.c. with the mirror shell 346 [AD2], the rms in the same interval of frequencies was 8.2 \AA .

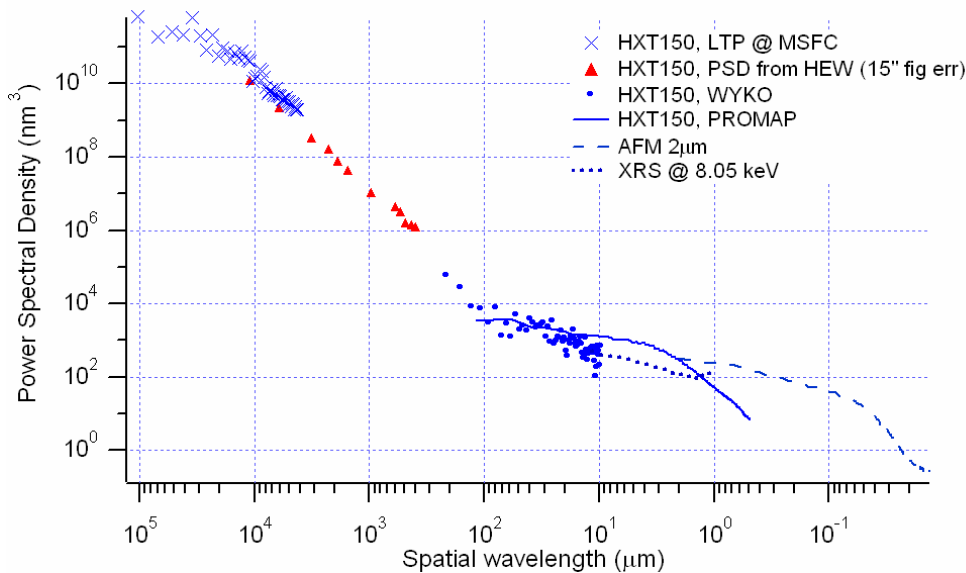



Fig. 10: overview of the roughness PSD of the surface of the HXT150, obtained with different methods of measurement. AFM, PROMAP, XRS, WYKO provide the PSD at high frequencies, the LTP covers the low frequencies. The gap between them is well bridged by the PSD inferred from the HEW trend (red triangles).

Some interesting topics from Fig. 10 can be remarked:

1. The PSD exhibits the typical profile with saturation at very low frequencies, followed by a power-law trend $P \propto f^{-n}$ with $n \sim 2.8$ (a very steep one, considering that the maximum allowed value for n is 3).


	<p align="center"><i>Multilayer Coatings for High-Energy Optics for Astrophysics</i></p> <p align="center">Results of tests performed at PANTER and INAF/OAB on the X-ray optic 349 manufactured at MSFC and Harvard-CfA</p>					
Code:02/07	INAF/OAB Technical Report	Issue:	1	Class	CONFIDENTIAL	Page: 14

- At shorter wavelengths than 100 μm a spectral break occurs. A clear “bump” is visible in the PSD. This is the roughness being seen in PROMAP, WYKO, AFM data. Note that a spectral slope could be detected also in the mirror shell 346 [AD2], at longer wavelengths (300 μm), and it was responsible for the HEW steep increase after 27 keV.

However, the integration of the all-measured PSD in the mentioned wavelengths interval 456 - 16 μm returns 8.5 \AA , lower than the 11.3 \AA requested by the HEW measurements. This deviation can be due to the uncertainty on the HEW measurement.

It is interesting now to remark some consequences on the HEW trend (Fig. 5):

- At low energies, the HEW trend increases very slowly as a consequence of the very steep decrease of the PSD.
- The contribution of the X-ray scattering is, however, non negligible even at very low energies: this can be seen from the difference of the HEW_{fig} value inferred from data (15 arcsec) vs. the value extrapolated from the HEW trend (25 arcsec, see Fig. 5).
- The cause of the large HEW also at low energies is probably the large roughness in the sub-millimeter range, down to some micron: the steep PSD at low frequencies, indeed, prevents the HEW from increasing.
- With the actual PSD and an incidence angle of 0.107 deg, we would expect to observe the HEW divergence after 38 keV. Obviously, this is not observed because the shell stops reflecting after 25 keV.

	<p style="text-align: center;"><i>Multilayer Coatings for High-Energy Optics for Astrophysics</i></p> <p style="text-align: center;">Results of tests performed at PANTER and INAF/OAB on the X-ray optic 349 manufactured at MSFC and Harvard-CfA</p>					
Code:02/07	INAF/OAB Technical Report	Issue: 1	Class	CONFIDENTIAL	Page: 15	

3. Optic 349 - HXT 230: results of tests at PANTER and INAF/OAB

The mirror shell HXT 230 has the same geometrical properties of the mirror shell 346 (see [AD2]). Just the spider obscuration is larger owing to the Al bars used to screen the spider against X-ray grazing incidence and consequent scattering. The difference is much less marked than for the case of HXT 150. The geometrical properties of the mirror shell are listed in Tab. 2.

Tab.2: geometrical parameters of the mirror shell HXT230.

<i>Parameter</i>	<i>symbol</i>	<i>value</i>
maximum mirror diameter (parabola)	$2R_{max}$	231.3 mm
median mirror diameter	$2R_{med}$	230.1 mm
minimum mirror diameter (hyperbola)	$2R_{min}$	226.4 mm
mirror length (parabola + hyperbola)	$2L$	426 mm
on-axis incidence angle	α	0.1638°
focal length (for a source at infinity)	f	10000 ± 3 mm
mirror walls thickness	τ	100 μm
Geometric cross-section from infinity	A	4.4 cm ²
Beam divergence (at mirror front-end)	θ	0.054°
Actual incidence angle on the parabola	α_{par}	0.218°
Actual incidence angle on the hyperbola (for <i>double reflection</i>)	α_{hyp}	0.110°
Actual image-mirror distance	X_i	10.9 m
<i>Lost</i> area fraction of parabola for double reflection	Q	49.6 %
Obscured area fraction by spider	V	10-14 %
Radius of the parabola single-reflection corona	r_p	41.9 mm
Radius of the hyperbola single-reflection corona	r_h	82.8 mm
Geometric cross-section for parabola single reflection, spider vignetted	A_G^{par}	2.51 cm ²
<i>Geometric cross-section for double reflection, spider vignetted</i> (1 keV)	A_G^{hp}	2.55 cm ²

3.1 – Witness mirror sample: X-ray reflectivity tests

For the witness multilayer sample the analysis was carried out with the BEDE-D1 diffractometer at INAF/OAB following the same methods exposed in Sect. 2.1 of [AD2]. The reflectance plot was analyzed by means of PPM [RD3], following the same fitting strategy: the experimental XRR angular scan at 8.05 keV (the Cu Kα1 X-ray line) and the fit results are shown in Fig. 11. The resulting thickness distribution is shown in Fig. 12.

Istituto Nazionale di Astrofisica (INAF) Via del Parco Mellini, 00100 Roma, Italy Osservatorio Astronomico di Brera (OAB) Via Brera 28, 20121 Milano, Italy Via E. Bianchi 46, 23807 Merate, Italy
--



Fig. 11: reflectance plot at 8.05 keV of multilayer witness mirror. Logarithmic plot. The agreement of data (red line) with model (blue line) is satisfactory.

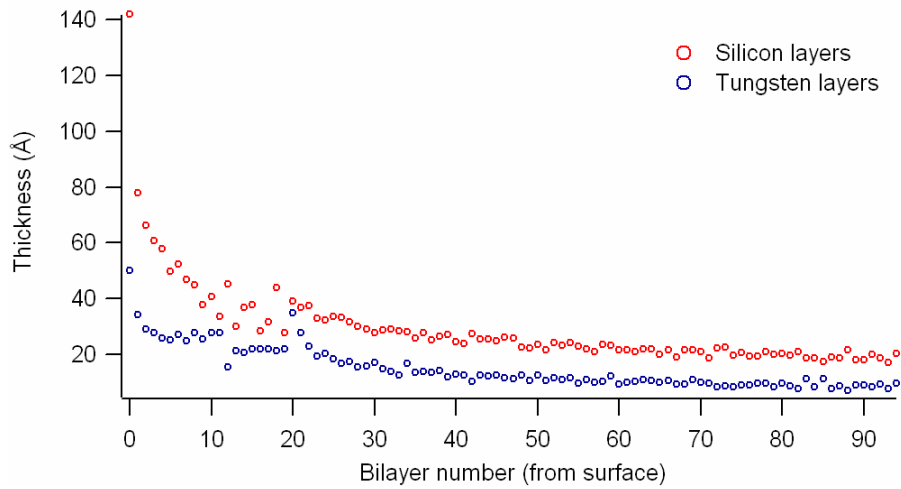



Fig. 12: thickness distribution for the W and Si layers for the multilayer deposited on the Witness sample. The random deviations superimposed to the power laws are significant at the boundary between the two power-law (bilayer n. 10-20).

Tab.3: inferred a,b,c parameters for the witness sample multilayer. The random deviations from the power laws are not considered.

	a (Å)	b	c	approx. d _{max} -d _{min}
1 st stack Si (20 bil.)	78.8	-0.90	0.26	143-36 Å
1 st stack W (20 bil.)	50.9	0.0	0.38	51-16 Å
2 nd stack Si (75 bil.)	70.4	6.37	0.30	39-19 Å
2 nd stack W (75 bil.)	30.4	-0.40	0.28	35-9 Å

	<p><i>Multilayer Coatings for High-Energy Optics for Astrophysics</i></p> <p>Results of tests performed at PANTER and INAF/OAB on the X-ray optic 349 manufactured at MSFC and Harvard-CfA</p>						
Code:02/07	INAF/OAB Technical Report	Issue:	1	Class	CONFIDENTIAL	Page:	17

The average roughness rms inferred from fit is 3.5 \AA , with a slight increase throughout the stack. The densities of W and Si should not differ too much from the natural values, even different density cannot be completely excluded. The parameters of the power-laws that best fit the thickness trend (excluding thereby the random oscillations of thickness) are listed in Tab. 3.

3.2 – PANTER results: effective areas

Some pn-EPIC fields derive from data are shown in Fig. 13, in energy-dispersive setup with the source set at 50 kV. A relevant amount of scattering is visible. A close view on the focal spot exhibits a quite symmetrical shape.

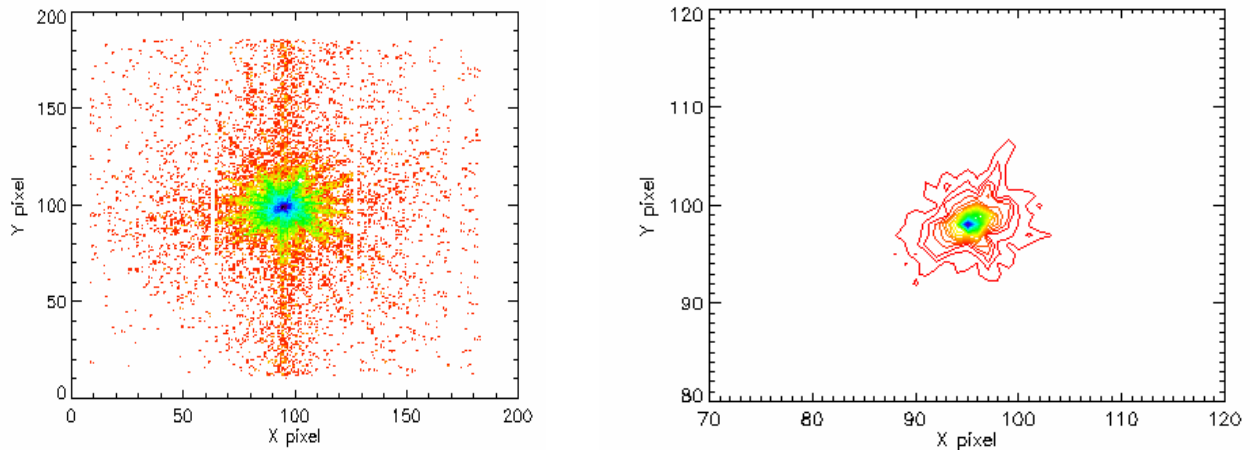


Fig. 13: the pn-EPIC field of the focal spot of the HXT230 mirror shell (20-37 keV). (left) log intensity map, (right) line contour plot.

For the measurement of EAs, we had at our disposal the monochromatic low energy sources (measured with the PSPC) and the high-energy exposures with the source at 20, 30, 50 kV, measured with the pn-EPIC. The EAs, measured in a circle of 250 arcsec radius (see Fig. 14) are fully consistent in the overlapping spectral regions. The EA plot is overplotted to the models with several possible roughness rms values (4- 20 \AA). The multilayer recipe has been changed with respect to that of the witness in order to better fit the peaks position (the d-spacing was reduced by 6 %). The measured values match well the model with a surface rms of 16 \AA in the energy range 15-25 keV, whereas at higher energies they are better fitted assuming 14 \AA down to 12 \AA as σ value. At low energies the measured effective areas underestimate all the theoretical models. This reduction of the needed roughness for increasing energies is commonly observed and can be explained as a reduction of the scattering angles for decreasing λ . From the intersection points models/experiment we can compute that the value $\sigma = 12 \text{ \AA}$ should be referred to surface wavelengths smaller than $6 \mu\text{m}$. This value is consistent with the surface PSD measurements (see Sect. 3.6).

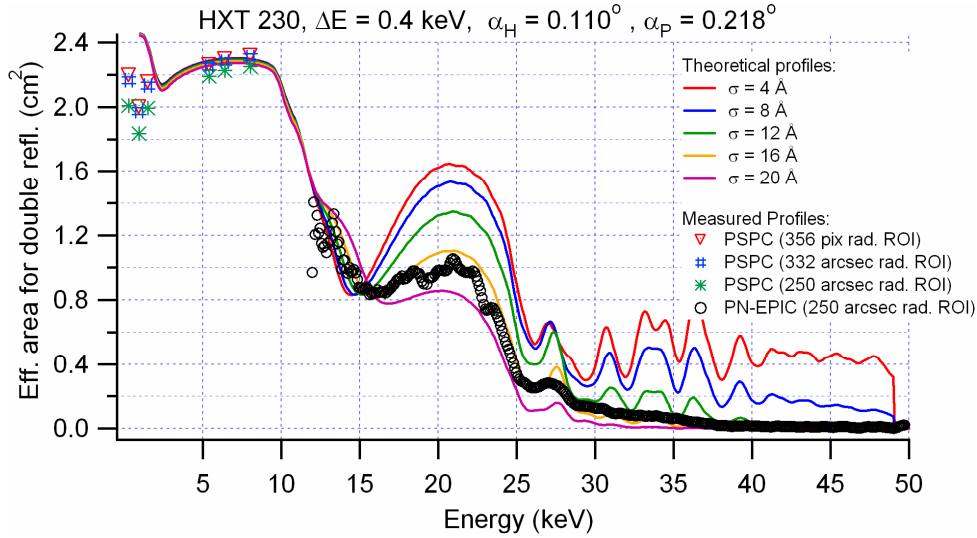



Fig. 14: mirror shell HXT 230 **effective area** (EA) of the mirror shell HXT 230 for double reflection as function of energy at the PANTER facility from 0.5 to 50 keV. Linear plot. A constant energy resolution of 0.4 keV is assumed.

3.3 – PANTER results: Half Energy Widths

Fig. 15 plots the measured HEW trend from PANTER images with PSPC and pn-EPIC. For PSPC data, the pixel size was subtracted in quadrature from data. For pn-EPIC data, the HEW values are computed by filtering the events within energy bands with 2 keV bandwidth and computing the Encircled Energy. The HEW is evaluated by interpolation of data reduce the effect of the finite size of pixels. The error bars are calculated by propagating the error – mainly due to the finite pixel size: moreover, as the spectrum can vary sensitively within the assumed bandwidth, the HEW are plotted versus the energy centroid in each bandwidth.

After an initial increase up to 6.4 keV, the HEW trend oscillates around 40 arcsec up to 29 keV, but it does not exhibit the divergence at 27 keV like the mirror shell 346 [AD2]. A sudden increase at 30 keV is followed by a plateau and then by a rapidly increasing trend around 37 keV. The HEW values in the common spectral regions of 20, 30, 50 keV are in agreement within 2 arcsec. The error in the HEW determination can be also estimated in 2 arcsec in the first “plateau” region.

As we will see in section 3.6, the measured PSD is able to explain the general trend of the HEW. The “jump” at 30 keV, however, would require a PSD peak at 150 μm spatial wavelength, which is *not* observed in WYKO data.

	<p><i>Multilayer Coatings for High-Energy Optics for Astrophysics</i></p> <p>Results of tests performed at PANTER and INAF/OAB on the X-ray optic 349 manufactured at MSFC and Harvard-CfA</p>				
Code:02/07	INAF/OAB Technical Report	Issue: 1	Class	CONFIDENTIAL	Page: 19

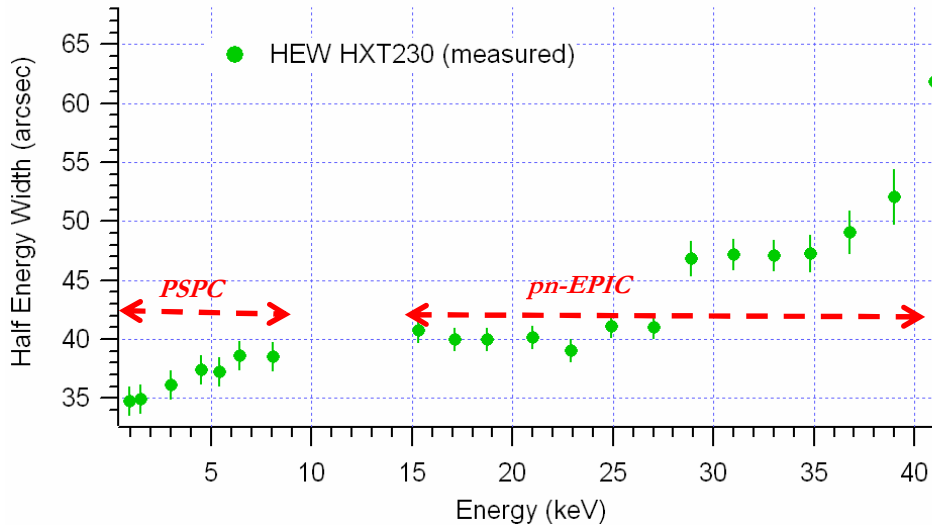


Fig. 15: the measured HEW trend of the mirror shell HXT 230 with both PSPC (low energies) and pn-EPIC (high energies). The detector spatial resolution of the PSPC was subtracted in quadrature from data. The finite pixel size of the pn-EPIC was ruled out by the interpolation of PSF data.

3.4 – X-ray tests at INAF/OAB

X-ray reflectivity and X-ray scattering tests were performed at INAF/OAB onto some pieces of the mirror shell, using the BEDE-D1 diffractometer in monochromatic setup. The reflectance plot at 8.05 keV is plotted in Fig. 16.

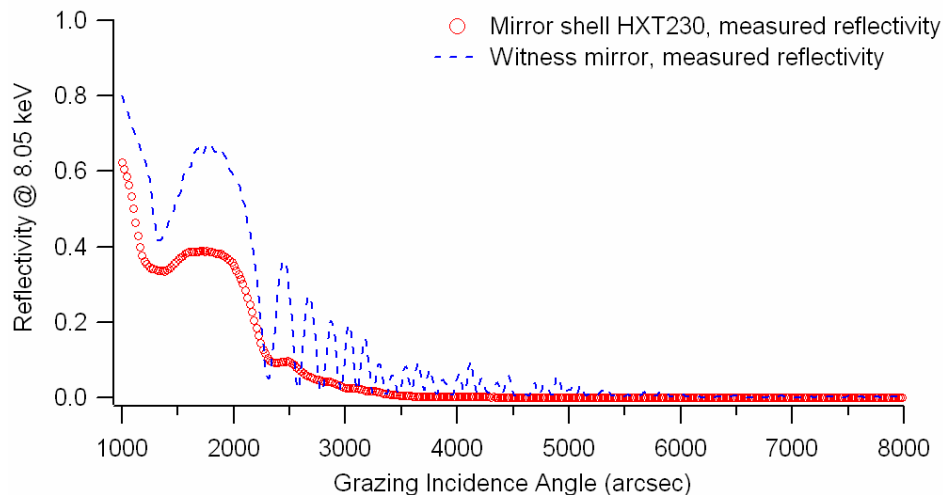



Fig. 16: XRR measurement onto a piece of shell HXT230. The reflectivity of the **Witness mirror** is also overplotted for comparison. Note the matching of peaks.

	<p><i>Multilayer Coatings for High-Energy Optics for Astrophysics</i></p> <p>Results of tests performed at PANTER and INAF/OAB on the X-ray optic 349 manufactured at MSFC and Harvard-CfA</p>						
Code:02/07	INAF/OAB Technical Report	Issue:	1	Class	CONFIDENTIAL	Page:	20

The geometrical deformation of the piece of shell under test (approx. 10 x 10 cm) did not allow a reliable measurement of the reflectivity at angles smaller than 1000 arcsec: at larger angles, the reflectivity pattern is similar to that of the witness (see Fig. 16), but it is consistent with a much larger surface roughness (12-16 Å), caused by a worse smoothness of the Nickel substrate. This rms roughness value is consistent also with the σ used to fit the PANTER data, even if the acceptance angle in use is 1200 arcsec, twice larger than at PANTER. An accurate inspection shows that the peaks of the shell XRR are slightly larger angles than that of the witness, indicating that the average d-spacing of the multilayer deposited on the shell is smaller (by 2% approx.). A different position of peaks is also observed in EAs measured at PANTER (Fig. 14).

The high level of roughness is also apparent from the XRS measurement performed at 8.05 keV at 1800 arcsec incidence angle (see Fig. 17). The scattered beam exhibits oscillations caused by the interference of scattered waves at each interface.

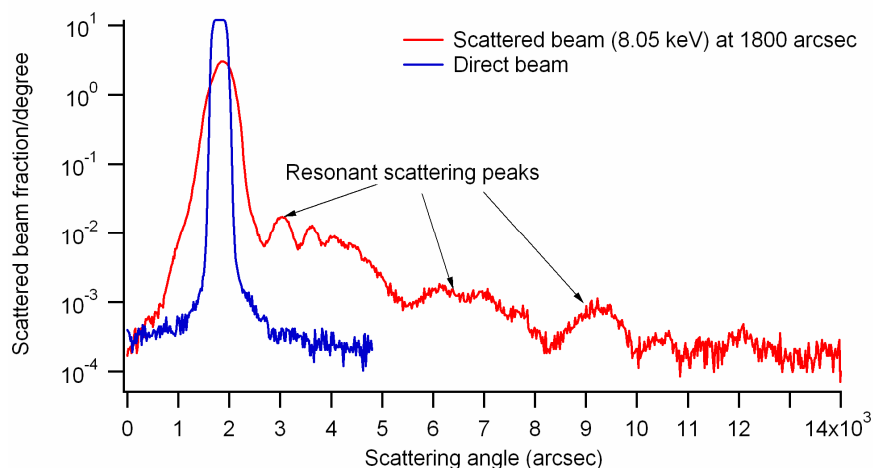



Fig. 17: XRS measurement onto a piece of shell HXT230. The coherent nature of the roughness throughout the stack is apparent from the complex structure of the scattering diagram.

3.5 – Topographical analysis (PROMAP, WYKO and AFM)

3.5.1 – PROMAP 40x

The topographical inspection with PROMAP 40x (performed at *Media-Lario techn.*, see Fig.17) highlights a smoother landscape than HXT150 in the spectral domain 150 – 0.2 μm (compare with Fig. 7). However, a large amount of “holes” are still present and the surface appears still undulated, even if many scratches are not visible. The surface topography has been analyzed in terms of PSD, after ruling out all the surface features higher than 50 nm (likely contaminations), along the y direction, i.e. the X-ray incidence plane. The computed PSD is plotted in Fig. 20.

	<p><i>Multilayer Coatings for High-Energy Optics for Astrophysics</i></p> <p>Results of tests performed at PANTER and INAF/OAB on the X-ray optic 349 manufactured at MSFC and Harvard-CfA</p>					
Code:02/07	INAF/OAB Technical Report	Issue: 1	Class	CONFIDENTIAL	Page: 21	

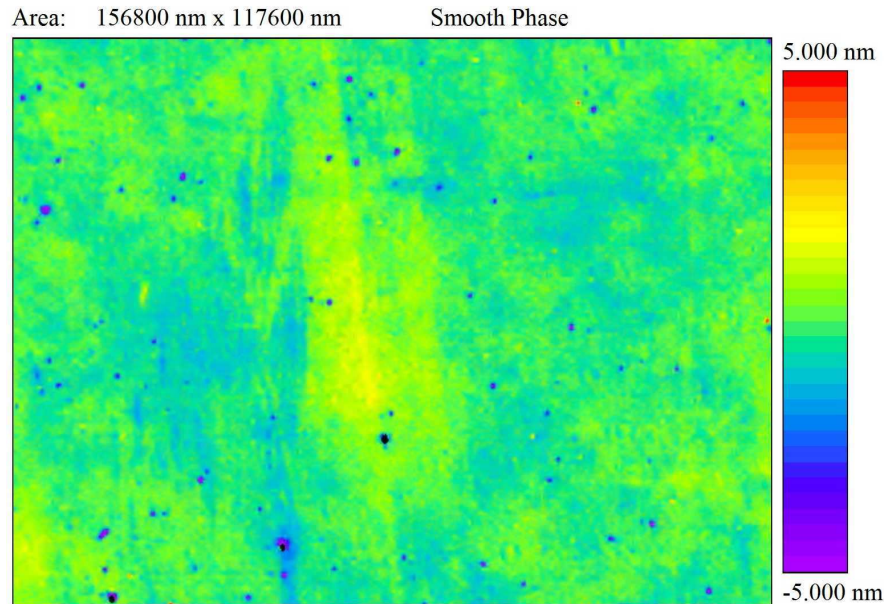


Fig. 17: a PROMAP40x image of the HXT230 flattened surface (courtesy by Media-Lario techn.). The surface appears smoother than the HXT150 (Fig. 7), without evident scratches. Holes are, indeed, still frequent.

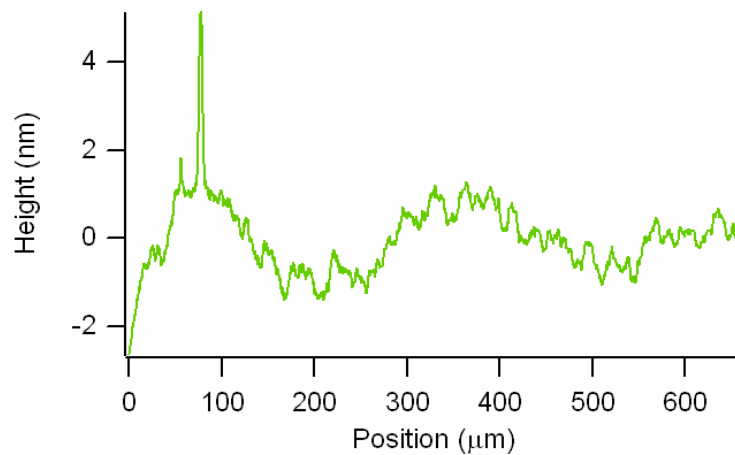



Fig. 18: a WYKO profile of a sample of the HXT 230 mirror shell, in the optical axis direction.

3.5.2 – WYKO 20×

Some profiles of the shell with WYKO 20x were also taken at INAF/OAB. The profiles exhibit a relevant high frequencies contents, with holes and peaks some nm high (see Fig. 18). The PSD, covering a spectral range from 300 down to 10 μm wavelengths, is consistent with the PROMAP measurement (see Fig. 20).

	<p align="center"><i>Multilayer Coatings for High-Energy Optics for Astrophysics</i></p> <p align="center">Results of tests performed at PANTER and INAF/OAB on the X-ray optic 349 manufactured at MSFC and Harvard-CfA</p>					
Code:02/07	INAF/OAB Technical Report	Issue: 1	Class	CONFIDENTIAL	Page: 22	

3.5.3 – AFM (2 μm)

Also the HXT230 mirror shell was sampled in the high frequency range by means of AFM measurements (performed at Media-Lario techn.). The derived PSD from AFM measurements cover the spectral range 2 μm - 15 nm. A 3D visualization of a sampled point is shown in Fig. 19: the average rms of the AFM measurements is 11.5 Å, in reasonable agreement with the PANTER EA values (see Fig. 14). The computed PSD is in good agreement with the PROMAP measurements.

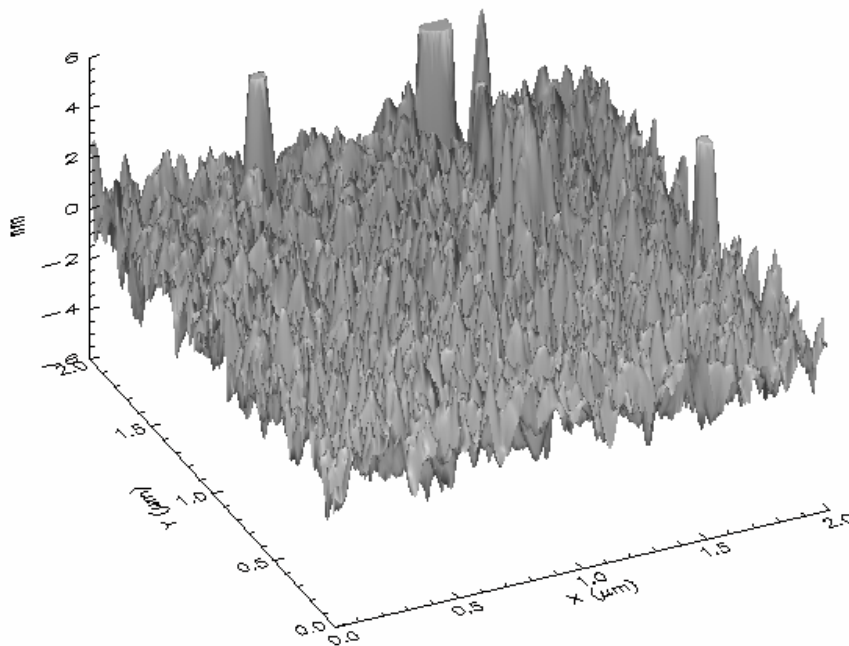



Fig. 19: a 2 μm AFM map of a point of the HXT230 (courtesy of Media-Lario techn.). The rms of this map is 10 Å..

3.6 – Final PSD - HEW trend interpretation

The PSD computed from the topographical techniques and from the analysis of the X-ray scattering measurements are plotted in Fig. 20. All the measurements are referred to the outer surface of the multilayer.

The medium and high-frequency range (300 – 0.03 μm) of the surface spectrum is fully characterized by the measurements performed on pieces of the mirror shell. The PSD, however, at very low frequencies is not known because no LTP measurement is available.

From the HEW trend we can derive the PSD in the wavelengths range 7 mm – 95 μm using the equations reported in Sect. 2.5 [RD4], neglecting the presence of the multilayer and the divergence of the incident X-ray beam. The computed PSD is overplotted in Fig. 20: in order to achieve a good matching with the PSD at higher frequencies, we assume $\text{HEW}_{\text{fig}} = 25$ arcsec. This value is close to the figure error value (26 arcsec) assumed for the mirror shell 346, with the same nominal shape and size

	<p><i>Multilayer Coatings for High-Energy Optics for Astrophysics</i></p> <p>Results of tests performed at PANTER and INAF/OAB on the X-ray optic 349 manufactured at MSFC and Harvard-CfA</p>						
Code:02/07	INAF/OAB Technical Report	Issue: 1	Class	CONFIDENTIAL	Page:	23	

[AD2], but in absence of LTP measurements it cannot be firmly established. Smaller values for HEW_{fig} (down to 20 arcsec) are also possible.

The PSD calculated from the HEW is in good agreement with the directly measured. Moreover, from the HEW we can also derive the rms of the surface in the spectral interval 77 – 7.4 μm . As discussed in [RD4], the upper wavelengths limit is set by the HEW *at the maximum energy being measured* whereas the lower wavelengths limit is determined by the radius of the ROI at the same energy. This required σ value is **4.6 Å**; *from the measured PSD we can easily compute the σ value in the same integration window, which returns 4.2 Å, in very good agreement with the HEW data*. It is worth noting that the integration in the same wavelengths range of the PSD for the mirror shell 346 [AD2] returned a larger value of $\sigma = 6.5 \text{ Å}$. This can be responsible for the quickly divergent HEW trend, that was observed in that case.

Some remarks on the PSD:

1. The low frequency regime is characterized by a steep decrease with a spectral index $n > 2.5$, which causes the low HEW increase in soft X-rays. On the other hand, it is also responsible for a relevant X-ray scattering also at low energies (Fig. 15). The PSD slope is even steeper in the spectral range 500 - 200 μm : this can be responsible for the HEW saturation at 15 keV $< E < 27 \text{ keV}$.
2. The HEW step at 30 keV (Fig. 15) can be justified by a sharp PSD peak at 150 μm , *not visible in the PSD computed from WYKO data*.
3. The PSD decays much more smoothly ($n \sim 1$) at high frequencies. This is consistent with an incoming increase like the one being observed from HEW data around 40 keV.
4. The integration of the PSD at wavelengths smaller than 6 μm returns **11.8 Å**, *in agreement with EA data as measured at PANTER (see Sect. 3.2)*.

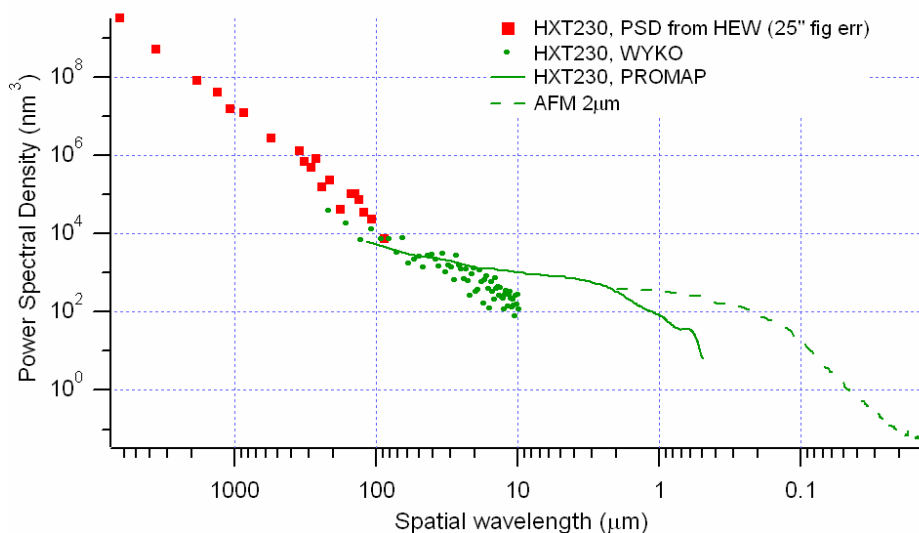



Fig. 20: the PSD of the mirror shell HXT 230. The PSD computed with different techniques are in good agreement. The PSD derived from the HEW trend is also overplotted.

		<p><i>Multilayer Coatings for High-Energy Optics for Astrophysics</i></p> <p>Results of tests performed at PANTER and INAF/OAB on the X-ray optic 349 manufactured at MSFC and Harvard-CfA</p>					
Code:02/07	INAF/OAB Technical Report	Issue:	1	Class	CONFIDENTIAL	Page:	24

4. Mirror shells HXT 150 + 230: overall optic properties

The characterization of the whole optic has also been performed, with both shutters open. The alignment of the optic has been changed, however, because the two shells well *confocal* but they are not exactly *coaxial*. In the two previous sections the characterization was performed in the best align conditions either for the HXT150 or HXT230 mirror shell, so the X-ray source was perfectly on-axis, but the alignment had to be changed, when switching from one shell to the other. With both shutters open, the two shells could not be kept aligned together and the measurement was performed in a trade-off position, after averaging the best alignment angular positions for the two shells.

The departure of the adopted configuration from the best alignment position is highlighted by the shape and the size of the single-reflection coronae, that are *not circular* and have not the radii values as listed in Tab. 1. Some pn-EPIC fields (Fig. 21) show clearly the situation: the shapes of the arcs of coronae are suitable, indeed, to measure precisely the shells misalignment (Sect. 4.1.2).

The good confocality of the two shells is evident from Fig. 21: the two contour plots exhibit only one bright nucleus (only slightly elongated in the vertical direction by 2-3 arcsec). However, up to energies 20-25 keV, the shape of the “wings” of the focal spot is quite circular, whereas at higher energies (26-40 keV) two lobes appear in the contour plot. The lobes orientation, as we shall soon see, the same of the plane located by the two optical axes. If the two foci were non-coincident, the lobes would be better seen at low energies, where the HEW is smaller. As the asymmetry appears better in the hardest band, the two lobes are probably caused by an enhancement of the XRS due to an increase of the incidence angle on one side of each mirror shell.

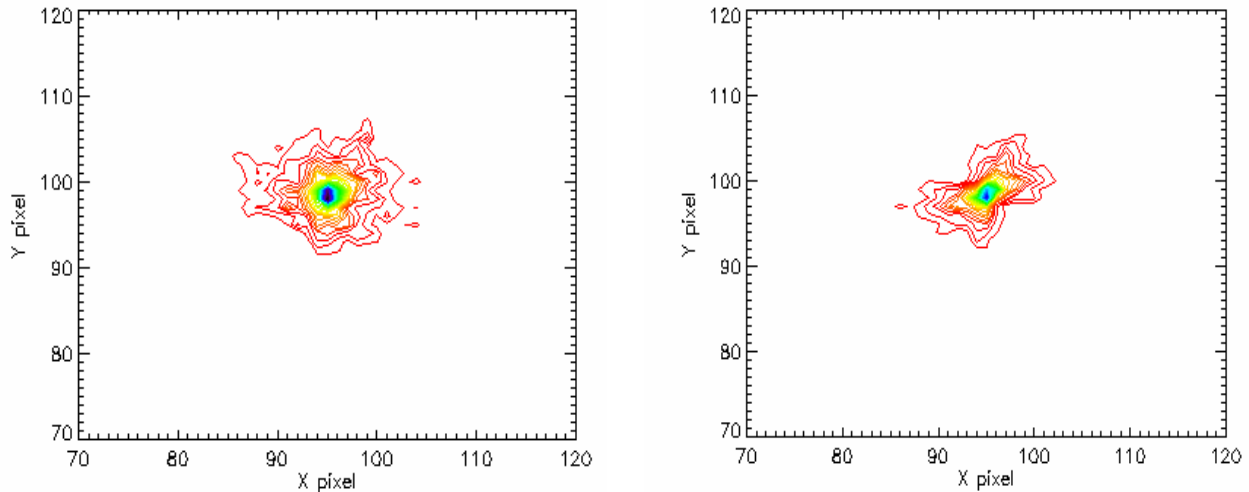



Fig.21: close views on the pn-EPIC fields of the exposure of the whole optic (150+230), contour plots. (left) 20-25 keV – (right) 26-40 keV: the two lobes lie roughly in the plane of the two optical axes.

	<p align="center"><i>Multilayer Coatings for High-Energy Optics for Astrophysics</i></p> <p align="center">Results of tests performed at PANTER and INAF/OAB on the X-ray optic 349 manufactured at MSFC and Harvard-CfA</p>					
Code:02/07	INAF/OAB Technical Report	Issue:	1	Class	CONFIDENTIAL	Page: 25

4.1 – PANTER results: effective areas

4.1.1 – Experimental results

The EA of the two mirror shells, measured with the usual methods, is plotted in Fig. 22 (marks). It is the superposition of effective areas measured at low energies in monochromatic setup (green asterisks) with the PSPC detector, plus the results of the energy-dispersive setup with the pn-EPIC detector and the X-ray continuum illumination with the X-ray source at the 20 and 50 kV voltage (black circles). Due to the closeness of a single-reflection corona to the focal spot (see Fig. 23), all the EA values were measured in a smaller ROI than for the previous measurements (**205 arcsec radius** vs 250). The measured EA data with the different X-ray sources biases are mutually consistent.

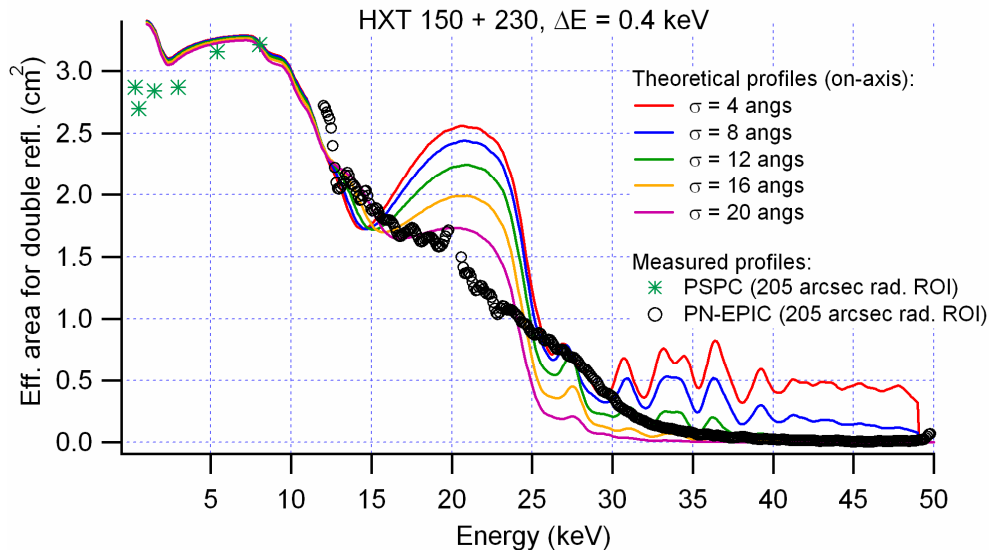



Fig.22: **effective area (EA)** for double reflection as a function of the energy at the PANTER facility from 0.5 to 50 keV. Measured data (marks) and theoretical model (lines). The models are simply the sum of the best-fit models for the mirror shells HXT150 and HXT230 for different σ values. The disagreement is apparent.

Experimental data are overplotted to theoretical models, that are simply obtained by summing the models for the EA of the HXT150 and HXT230 mirror shells (see Sect. 2.1 and 3.2), for variable values of the roughness. It is apparent that the models cannot explain the smooth decrease of the EA for increasing photon energy, without the peaks and the cut-off that should be expected from the contributions of the two mirror shells. We find a possible explanation of the discrepancy in the next subsection.

4.1.2 – Interpretation of effective areas

As already mentioned, the best alignment of mirror shell HXT 150 differed from that of HXT 230, even if the two foci were coincident in all X-rays measurements. For the X-ray characterization of the whole optic we could not align both shells simultaneously, we have thereby chosen the average of the best-

		<p><i>Multilayer Coatings for High-Energy Optics for Astrophysics</i></p> <p>Results of tests performed at PANTER and INAF/OAB on the X-ray optic 349 manufactured at MSFC and Harvard-CfA</p>					
Code:02/07	INAF/OAB Technical Report	Issue: 1	Class	CONFIDENTIAL	Page: 26		

alignment rotation/tilt angular coordinates of the two, individual shells. Since the X-ray source is seen off-axis by *both* shells, X-rays impinge with variable incidence angles on different points of both shells: therefore, the reflectivity of different mirror points varies, and the same does the EA.

The first step consists of an accurate misalignment estimation along with the shape and the size of single-reflection coronae. In Fig. 23 we report the same pn-EPIC field of the focal spot in 50 kV measurement setup: three visible single-reflection coronae are visible: the smallest one (Fig. 23, left) is due to the reflection on the HXT150 parabola, the average-size corona (Fig. 23, left) to the hyperbola of HXT 150, the largest one (Fig. 23, right) is the parabola of the HXT 230. The shapes of these coronae are functions of the rotation/tilt optic angles: the best fit is reached by adopting the values in Tab. 4.

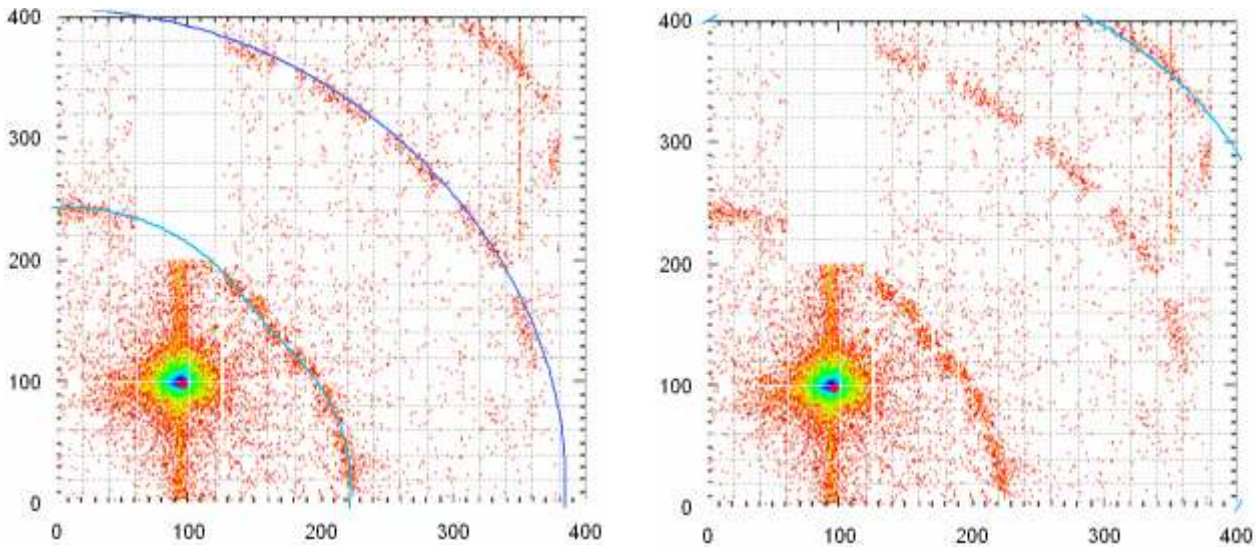



Fig. 23: single-reflection coronae in the pn-EPIC field with the source at 50 kV, with both shutters open: the shapes and the sizes of the single reflection can be used to measure precisely the misalignment of the two mirror shells with respect to the trade-off adopted for the measurement. (left) simulation of the single reflection coronae of the HXT 150: parabola (bright blue) and hyperbola (dark blue). (right) simulation of single reflection coronae for the HXT 230: only a small arc of the single reflection on the parabola is visible in the pn-EPIC field.

Tab.4: misalignment of the two shells with respect to the trade-off position for measurement with both shutters open, as derived from the single reflection coronae pattern of Fig. 22

	rotation (arcsec)	tilt (arcsec)	overall misalignment (arcmin)
HXT 150	-115	+92	2.45
HXT 230	+83	-80	1.91

In the second step, we divided the shells by intersecting them with a number (N=20) of meridional planes and computed the incidence angles of each sector for a $\omega \sim 2$ arcmin misalignment. The result is an uniform distribution of incidence angles lying between $\alpha_{\text{par}} - \omega$ and $\alpha_{\text{par}} + \omega$ for the parabola. After the first reflection, a fraction of the beam is reflected also by the hyperbola and only the

	<p style="text-align: center;"><i>Multilayer Coatings for High-Energy Optics for Astrophysics</i></p> <p style="text-align: center;">Results of tests performed at PANTER and INAF/OAB on the X-ray optic 349 manufactured at MSFC and Harvard-CfA</p>					
Code:02/07	INAF/OAB Technical Report	Issue: 1	Class	CONFIDENTIAL	Page: 27	

photons reflected *twice* are counted around the focal spot: the corresponding incidence angles on the hyperbola can be assumed to lie approximately in the range $\alpha_{\text{hyp}} + \omega$ and $\alpha_{\text{hyp}} - \omega$. With these incidence angles in hand, we can compute the reflectance R of each sector.

We can now calculate the EA for a double reflection:

$$A_e = \sum_{k=-N/2}^{k=+N/2} A_{e,k} (1 - Q_k) R(\alpha_{\text{par}} + k\omega/N) R(\alpha_{\text{hyp}} - k\omega/N),$$

the coefficients $A_{e,k}$ represent the geometric cross-section for the k -th sector of parabola (average radius R). Due to the variable incidence angle with k , it is not simply an N th fraction of the geometric cross-section of the parabola:

$$A_{e,k} = 2\pi RL \sin(\alpha_{\text{par}} + k\omega/N),$$

and the coefficients Q_k account for the rays that miss the hyperbola after being reflected by the parabola:

$$1 - Q_k = \frac{\sin(\alpha_{\text{hyp}} - k\omega/N)}{\sin(\alpha_{\text{par}} + k\omega/N)}.$$

The result is interesting: as in the EA expression only the product $(1 - Q_k)A_{e,k}$ appear, the most important terms in the sum are those with $k < 0$, i.e those with the smaller incidence angle on the parabola, even if the cross-section of parabola sector are smaller. Also the reflectivity of the parabola is enhanced by a reduction of the incidence angle, whilst the contrary occurs with the hyperbola.

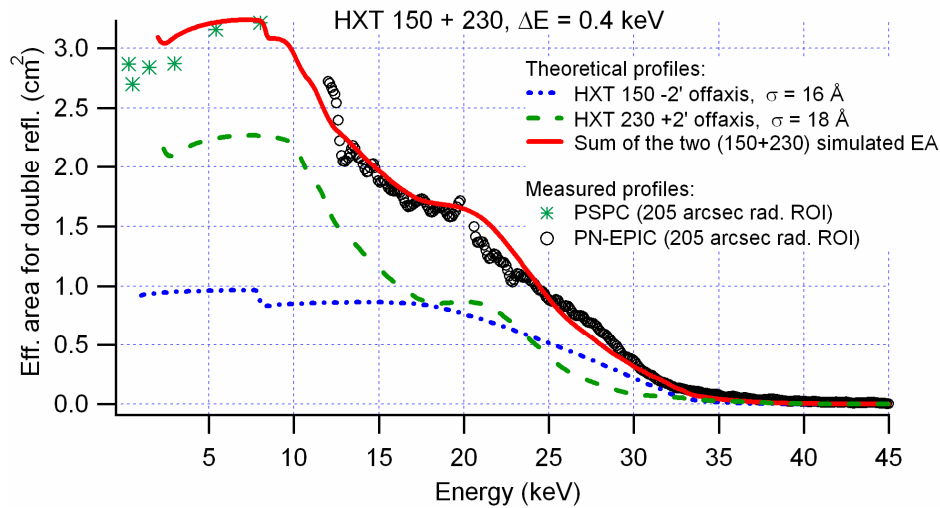



Fig. 24: the off-axis simulation of the EA for the 150+230 optic. The sum of the two simulated areas (red line) assuming the misalignments (Tab. 4) with respect to the PANTER axis is in good agreement with the experimental results (marks)

	<p><i>Multilayer Coatings for High-Energy Optics for Astrophysics</i></p> <p>Results of tests performed at PANTER and INAF/OAB on the X-ray optic 349 manufactured at MSFC and Harvard-CfA</p>						
Code:02/07	INAF/OAB Technical Report	Issue: 1	Class	CONFIDENTIAL	Page:	28	

The result of the computation is shown in Fig. 24: the dotted line is the off-axis area of the HXT150, and the dashed line that of the HXT230, simulated using the formulae above. Notice that the EA of the two mirror shells are more “spread” over the energy scale (e.g. the HXT150 reflects up to 32 keV) and the peak of the HXT230 is much less marked, with respect to the on-axis areas (see Figs. 4, 14, 22).

Now, the sum of the two off-axis areas (the red, solid line) matches quite well the experimental EA curve. The values of σ that best match the model to the experiment are 16 Å for the HXT150 and 18 Å for the HXT230, somehow larger than the ones we assumed for the fit of effective areas of the two single shells. This can be due to the smaller ROI adopted for the measurement, that excludes a relevant fraction of scattering from the focused photons count.

The residual discrepancies are of the order of the departures model/experiment already observed in the on-axis models (Figs. 4 and 14). Moreover, the modelization could be made more quantitative by computing exactly the incidence angles over the different sectors of the mirror shells (rather than assuming a linear variation). It should be remembered, in addition, that this approach would not be valid if the misalignment were larger than the smallest actual incidence angle on the parabola (8.6 arcmin), because additional vignetting effects should be taken into account.

4.2 – PANTER results: Half Energy Widths

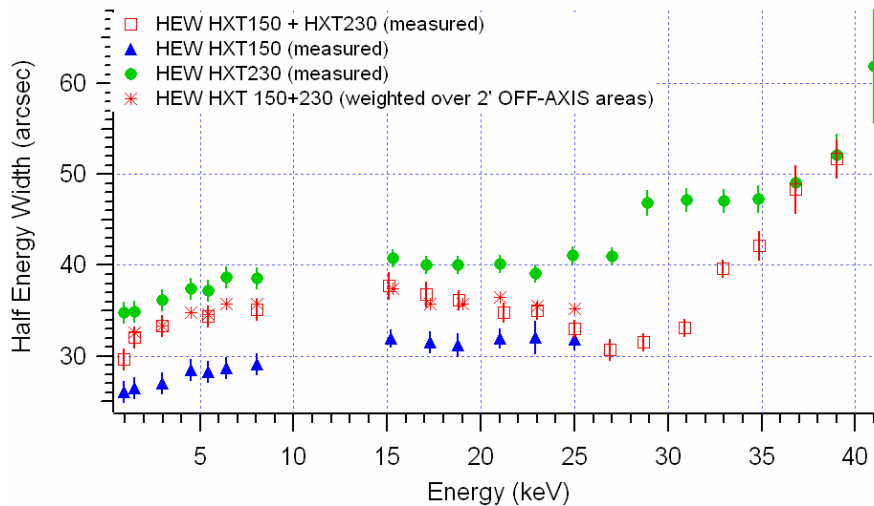



Fig. 25: the measured HEW of the 150+230 optic (squares) as compared with the HEW of the two single shells. The average of the single shells HEW, weighted over the off-axis EA, is also overplotted (red asterisks).

The HEW trend of the two mirror shell together appears to be intermediate between the two mirror shell separately, as expected. The agreement is also quantitative: in Fig. 25 we report the comparison between the measured HEW of the optic 150+230 and the average of the HEW of the two shells, weighted (as a 0th-order approximation) over the *actual* effective areas of the two shells:


	<p style="text-align: center;"><i>Multilayer Coatings for High-Energy Optics for Astrophysics</i></p> <p style="text-align: center;">Results of tests performed at PANTER and INAF/OAB on the X-ray optic 349 manufactured at MSFC and Harvard-CfA</p>					
Code:02/07	INAF/OAB Technical Report	Issue:	1	Class	CONFIDENTIAL	Page: 29

$$HEW_{150+230} = \frac{EA_{150} HEW_{150} + EA_{230} HEW_{230}}{EA_{150} + EA_{230}}.$$

The EAs have already being computed in the section 4.1.2 accounting for a misalignment of 2 arcmin for each shell. The agreement between the average and the experimental values is satisfactory at all the energies up to 25 keV. Over 27 keV the effective area of the HXT 150 drops quickly, therefore (also in absence of HEW/EA data over 27 keV for the HXT 150), one should expect that the HEW of the overall optic should be identical with the HXT 230 alone. The HEW is observed instead to diminish up to the energy of 30 keV, afterwards it starts to be increased up to reaching the level of the HXT 230 after 37 keV. In other words, the HEW increase (that could be related to a slope change of the PSD) is postponed with respect to the HXT 230.

This strange behaviour can have two *possible (not quantitatively verified)* explanations:

1. the ROI adopted for measurement is smaller, hence an important fraction of X-ray scattering can be lost at energies where the PSD bump scatters at angles between 205 and 250 arcsec from the focus;
2. even if we have no HEW measurement of the HXT150 beyond 25 keV (see Fig. 25) due to the cut-off of the total reflection of Nickel, we can infer from the measured PSD (see Sect 2.5) that ***the HEW of the HXT 150 should remain more or less constant up to 38 keV***. Were the EAs of the HXT150 those of Fig. 4, the contribution of the HXT150 would be negligible in the weighted sum. But *since in the adopted positioning of the shell the HXT150 has a larger EA than the HXT230* (see Fig. 25) *between 25 and 32 keV*, the lower HEW of the HXT150 almost dominate the weighted sum, ***yielding the minimum observed at 29 keV***, where the difference of the two areas is largest.

		<p><i>Multilayer Coatings for High-Energy Optics for Astrophysics</i></p> <p>Results of tests performed at PANTER and INAF/OAB on the X-ray optic 349 manufactured at MSFC and Harvard-CfA</p>					
Code:02/07	INAF/OAB Technical Report	Issue:	1	Class	CONFIDENTIAL	Page:	30

5. A comparison of the optics PSD and HEW

5.1 Optics 346 (HXT230) and 349 (HXT150 and HXT230)

In this section we summarize the results of the last characterizations. We plot in Fig. 26 and 27 the PSD, as derived from different techniques, for the optics 346 [AD2] and 349. The low ($f < 0.01 \mu\text{m}^{-1}$) and high ($f > 0.01 \mu\text{m}^{-1}$) frequencies (the distinction is purely conventional) have been separated for reader's comfort.

The comparison shows that:

1. The optic **346 is smoother** than both shells of the 349 **at the low frequencies**, whereas the two mirror shells HXT150 and 230 of the optic 349 have similar roughness levels (Fig. 26). This can be the reason why the HEW of the 349 is larger than that of the 346 at low energies: 34 arcsec (349 HXT230) vs 26 (346), at 0.5 keV.
2. The optic **346 is rougher** than both shells of the 349 **at the medium-high frequencies** ($0.01 - 1 \mu\text{m}^{-1}$), see Fig. 27. This causes a much larger HEW at high energies: 80 arcsec (346) vs 45 (349 HXT230), at 35 keV.
3. The shell **HXT150 of the optic 349 is rougher** than the HXT230 **at very high frequencies** ($f > 10 \mu\text{m}^{-1}$ Fig. 27): however, due to the small incidence angle and due to the limited size of the ROI used to compute the HEW, this part of the PSD causes a scattering out of the ROI and does not affect the HEW at the energies considered in the measurements (it affects, indeed, the EAs).

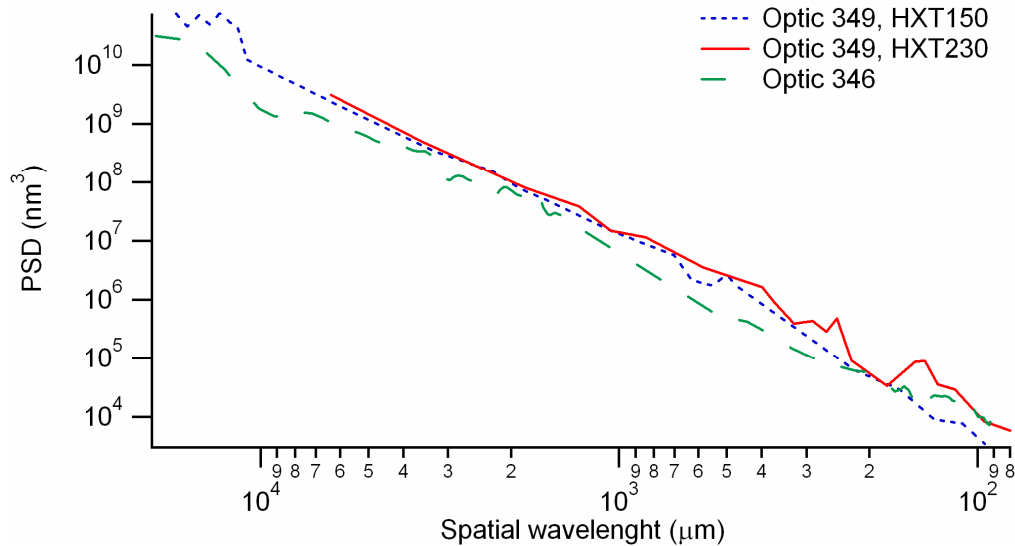


Fig. 26: a comparison of the low-frequency regime for the optic 346 and 349 (HXT150 and HXT230). The optic 346 is smoother, yielding a smaller X-ray scattering at low energies.

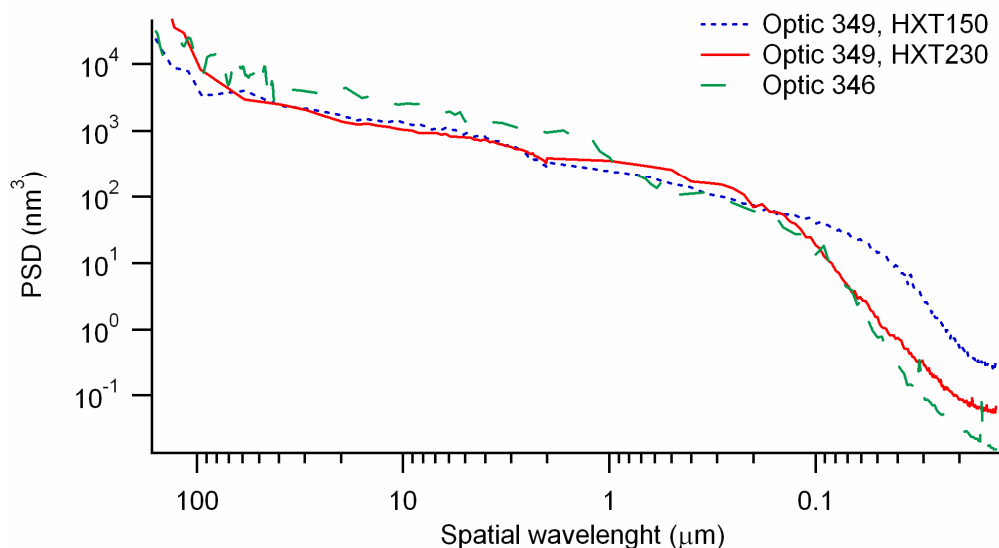


Fig. 27: a comparison of the high-frequency regime for the optic 346 and 349 (HXT150 and HXT230). The optic 346 is rougher, causing a larger HEW at high energies.

5.2 Comparison of HXT230 mirror shells (335, 346, 349 HXT230)

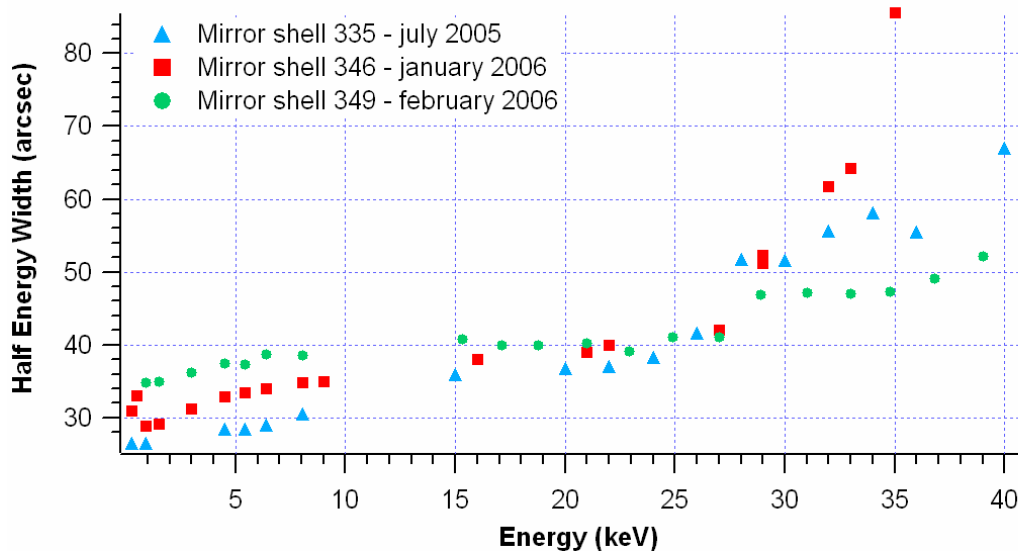



Fig.29: the different HEW trend for some mirror shells with the same incidence angle (0.164 deg) as measured at PANTER since July 2005.

		<p><i>Multilayer Coatings for High-Energy Optics for Astrophysics</i></p> <p>Results of tests performed at PANTER and INAF/OAB on the X-ray optic 349 manufactured at MSFC and Harvard-CfA</p>					
Code:02/07	INAF/OAB Technical Report	Issue:	1	Class	CONFIDENTIAL	Page:	32

In Fig. 29 we can see a comparison among three mirror shells manufactured at MSFC with the same on-axis incidence angle (0.164 deg). The best results achieved are *the 335 at low energies* and *the 349 (HXT230) at high energies*. The 346 has an intermediate behaviour at low energies whereas it exhibits the worst HEW trend at high energies.

Interestingly, all the HEWs are similar between 15 and 25 keV. All the increases of the HEW start around 27 keV, with more or less steep trends: the sudden “jumps” of the HEW, followed by a plateau, can be a marker of a PSD peak (see Fig. 26, near 150 μm), i.e. of a periodicity in the topography of the reflecting surface. However, due to the X-ray source divergence, the HEW jump would be smeared out unless they are broader than they were supposed.

No topographical measurement is available for the 335, hence no comparison can be performed on the PSD computed from its HEW trend (Fig. 29). In Tab. 5 we list some values of the roughness rms in similar spatial frequency windows. The comparison shows how small variations in the roughness at high frequency can make the difference (Fig. 29), especially at high photon energies. E.g., the 335 and the 349 have similar rms, but for the 335 it is more concentrated at high frequencies: therefore, it has a larger impact on the HEW in hard X-rays.

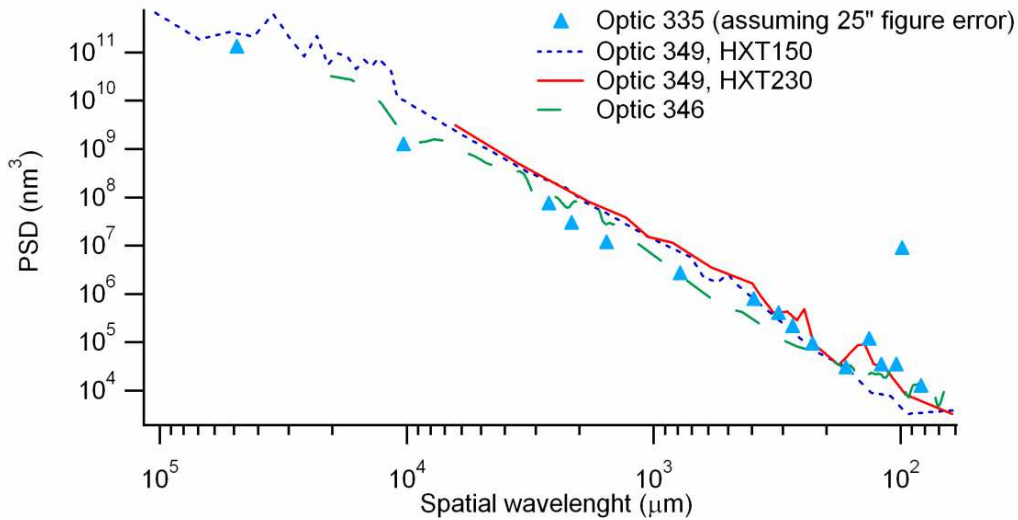


Fig. 30: comparison of the low-frequencies regime PSD for the mirror shells 335, 346, 349 (HXT230). In addition, the rms of the 335 in the spectral window 70- 7 μm should be 4.6 \AA to return the observed HEW trend.

Tab. 5 : comparison of some mirror shell rms values in the medium-high frequencies regime.

Optic (HXT 230)	σ value
335	(70 \div 7 μm): 4.6 \AA
346	(77 \div 7 μm): 6.5 \AA
349	(77 \div 7 μm): 4.4 \AA